Accepted Manuscript

Radiolytic alteration of biopolymers in the Mulga Rock (Australia) uranium deposit

Caroline M.B. Jaraula, Lorenz Schwark, Xavier Moreau, Walter Pickel, Leon Bagas, Kliti Grice

PII: S0883-2927(14)00275-3
DOI: http://dx.doi.org/10.1016/j.apgeochem.2014.11.012
Reference: AG 3365

To appear in: *Applied Geochemistry*

Please cite this article as: Jaraula, C.M.B., Schwark, L., Moreau, X., Pickel, W., Bagas, L., Grice, K., Radiolytic alteration of biopolymers in the Mulga Rock (Australia) uranium deposit, *Applied Geochemistry* (2014), doi: http://dx.doi.org/10.1016/j.apgeochem.2014.11.012

Radiolytic alteration of biopolymers in the Mulga Rock (Australia) uranium deposit

Caroline M.B. Jaraula [a,*], Lorenz Schwark [a,b*], Xavier Moreau [c], Walter Pickel [d], Leon Bagas [e] and Kliti Grice [a,*]

[a] Western Australia-Organic and Isotope Geochemistry Centre, Department of Chemistry, Curtin University, Bentley, Western Australia, 6102 Australia. C.Jaraula@curtin.edu.au; carolinejaraula@gmail.com; K.Grice@curtin.edu.au; Lorenz.Schwark@curtin.edu.au

[b] *Institute for Geosciences, Christian-Albrechts-University zu Kiel, D-24118 Kiel, Germany. ls@gpi.uni-kiel.de*

[c] *Energy and Minerals Australia, Ltd, 25 Richardson St, West Perth, Western Australia, 6005 Australia. XMoreau@eama.com.au*

[d] *Coal and Organic Petrology Services Pty Ltd, P.O. Box 174, Sans Souci, NSW, 2219 Australia. Walter.pickel@organicpetrology.com*

[e] *Centre for Exploration and Targeting, Crust to Core Fluids Systems, The University of Western Australia, 35 Stirling Highway, Crawley, Western Australia, 6009 Australia. Leon.bagas@uwa.edu.au*

* Corresponding authors: *C.Jaraula@curtin.edu.au, carolinejaraula@gmail.com +63 (2) 9275-42-5900; ls@gpi.uni-kiel.de +49(431) 880-2850; K.Grice@curtin.edu.au +61 (8) 9266-2474*

Keywords: radiolysis, radiolytic cracking, alkanones, degradation, peats, lignite

Abstract

We investigated the effect of ionizing radiation on organic matter (OM) in the carbonaceous uranium (U) mineralization at the Mulga Rock deposit, Western Australia. Samples were collected from mineralized layers between 53 to 58.5 m depths in the Ambassador prospect, containing <5300 ppm U. Uranium bears a close spatial relationship with OM, mostly finely interspersed in the attrinite matrix and *via* enrichments within liptinitic phytoclasts (mainly sporinite and liptodetrinite). Geochemical analyses were conducted to: (i) identify the natural sources of molecular markers, (ii) recognize relationships between molecular markers and U concentrations and (iii) detect radiolysis effects on molecular marker distributions. Carbon to nitrogen ratios between 82 and 153, and Rock-Eval pyrolysis yields of 316 to 577 mg hydrocarbon/g TOC (HI) and 70 to 102 mg CO_2/g TOC (OI) indicate a predominantly lipid-rich terrigenous plant OM source deposited in a complex shallow swampy wetland or lacustrine environment. Saturated hydrocarbon and ketone fractions reveal molecular distributions co-varying with U concentration. In samples with <1700 ppm U concentrations, long-chain *n*-alkanes and alkanones (C_{27} to C_{31}) reveal an odd/even carbon preference indicative of extant lipids. Samples with ≥1700 ppm concentrations contain intermediate-length *n*-alkanes and alkanones, bearing a keto-group in position 2 to 10, with no carbon number preference. Such changes in molecular distributions are inconsistent with diagenetic degradation of terrigenous OM in oxic depositional environments and cannot be associated with thermal breakdown due to the relatively low thermal maturity of the deposits (R_r = 0.26 %). It is assumed that the intimate spatial association of high U concentrations resulted in breakdown *via* radiolytic cracking of recalcitrant polyaliphatic macromolecules (spores, pollen, cuticles, or algal cysts) yielding medium chain length *n*-alkanes (C_{13} to C_{24}). Reactions of *n*-alkenes with OH^- radicals from water hydrolysis produced alcohols that dehydrogenated to alkanones or through

carbonylation formed alkanones. Rapid reactions with hydroxyl radicals likely decreased the isomerization of *n*-alkenes and decreased alkanone diversity, such that the alkan-2-one isomer is predominant. This specific distribution of components generated by natural radiolysis enables their application as "radiolytic molecular markers". Breaking of C-C bonds through radiolytic cracking at temperatures much lower than the oil window (<50º C) can have profound implications on initiation of petroleum formation, paleoenvironmental reconstructions, mineral exploration and in tracking radiolysis of OM.

1. INTRODUCTION

The evolution of many uranium (U) deposits can be closely linked to organic matter (OM), particularly those hosted by peat and lignite (e.g.; Halbach et al., 1980; Ilger et al., 1987; Spirakis, 1996a; Alexandre and Kyser, 2006). The association of uranium with OM-rich deposits in other sedimentary environments are also documented (e.g. Breger, 1974; Idiz et al., 1986; Disnar and Sureau, 1990). It has been reported that OM plays a role in: (i) concentrating uranium through sorption; (ii) forming stable complexes; and (iii) involving reduction-oxidation (redox) changes of uranyl species. In systems where temperatures remain below 50° C, reduction of aqueous soluble U [VI] to less soluble U [IV] is a relatively slow process, however microbially-mediated processes and catalysis by clay minerals are kinetically favoured (e.g. Anderson, 1987; Goldhaber et al., 1987; Landais et al., 1987; Nakashima et al., 1984; Lovely et al., 1991; Nakashima et al., 1999; Behrends and Van Cappellen, 2005; Jeon et al., 2005).

A carbonaceous uranium and multi-element deposit, referred to as "Mulga Rock" from Western Australia (Fig. 1a), is hosted in mid-Eocene lignite, peat, carbonaceous sandstone and shale (Douglas et al., 2011). Uranium at Mulga Rock bears a close relationship with OM and this provides important clues to the interaction between OM, uranium deposition, and the

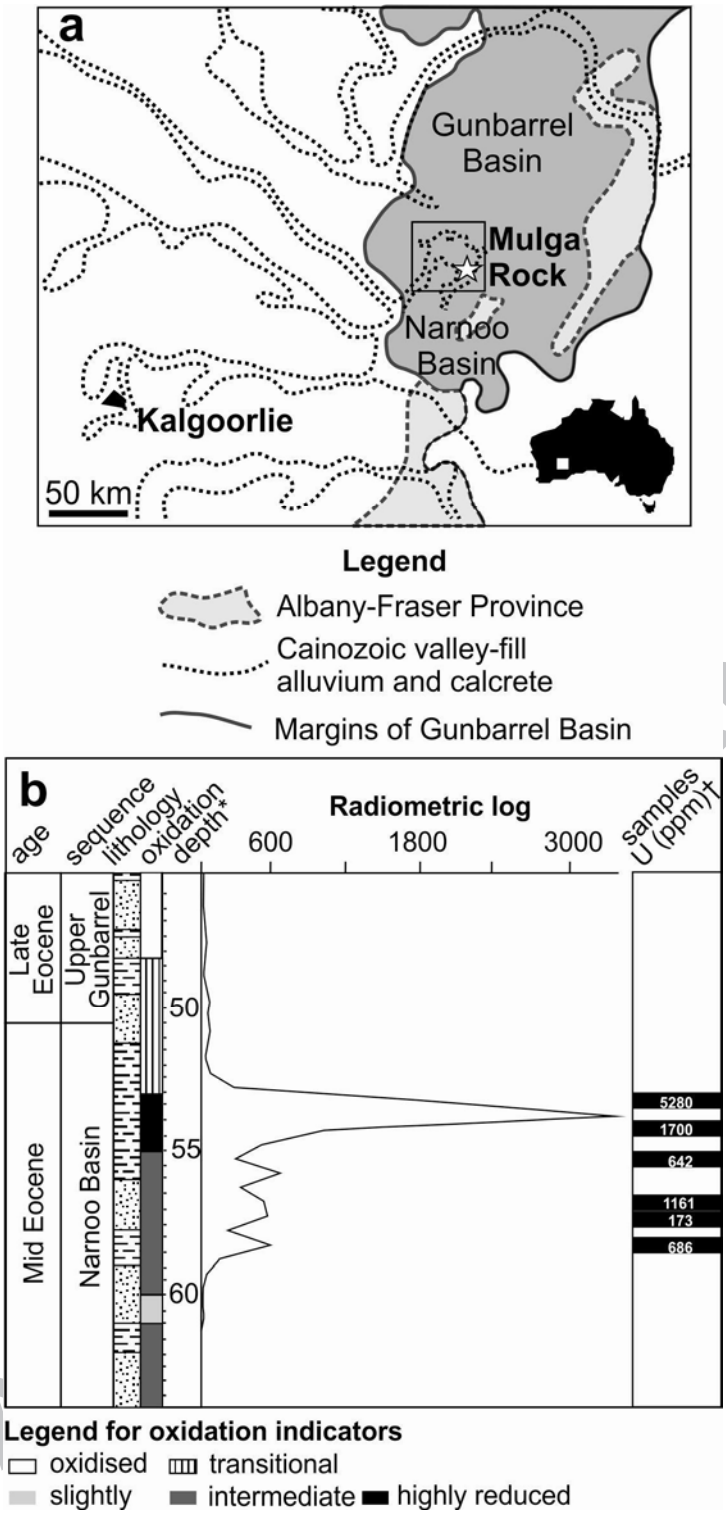
a
Gunbarrel Basin
Mulga Rock
Narnoo Basin
Kalgoorlie
50 km
Legend
Albany-Fraser Province
Cainozoic valley-fill alluvium and calcrete
Margins of Gunbarrel Basin
b
age
sequence
lithology
oxidation
depth*
Radiometric log
600
1800
3000
samples U (ppm)†
Late Eocene
Upper Gunbarrel
Mid Eocene
Narnoo Basin
50
55
60
5280
1700
642
1161
173
686
Legend for oxidation indicators
oxidised
transitional
slightly
intermediate
highly reduced

Figyre 1

effect of ionizing radiation on the OM. In our study of this deposit, we aim to: i) recognize the natural sources of molecular biomarkers; ii) identify relationships between molecular biomarkers with uranium accumulations; and iii) detect radiolysis effects on molecular distributions. This approach has been recognised, but it has not been overly exploited for its potential applications to tracking radiolysis, for uses in petroleum and mineral exploration, and for understanding the mechanisms leading to the formation of low-temperature uranium ore in carbonaceous deposits (Landais et al., 1987; Forbes et al., 1988; Landais, 1996a; Gizė, 2000; Greenwood et al., 2013). Here we show that the biologically associated distributions of saturated and polar hydrocarbons from samples with low uranium concentrations are distinct from those associated with mineralized deposits having at least 1700 ppm U concentrations. We ascribe this difference from the results of ionizing radiation with immobilization of uranium and its daughter products into the highly aliphatic phytoclasts and very fine organic matrix of carbonaceous mud at Ambassador. We propose the term “radiolytic molecular markers” to distinguish products resulting from the mechanism of cleaving due to ionizing radiation rather than from those due to thermal cracking or microbial oxidation.

1.1 Radiolysis

The chemical alteration that results from exposure to radioactive materials is radiolysis (Meunier et al., 1990). Resulting products of radiolysis can mask the original molecular composition. Alteration of organic matter exposed to ionizing radiation manifests in various ways, and these can be studied through different analytical techniques. In petrographic analysis, vitrinite reflectance increases (Breger, 1974) and complexly zoned haloes form in the organic matrix around U-bearing minerals (Leventhal, 1987). Bulk elemental analyses revealed a decrease in H/C and increase in O/C (Landais et al., 1987; Kříbek et al., 1999; Court et al., 2006).

The bitumen yield decreases and is ^{13}C enriched (Dahl et al., 1988; Landais, 1993; Leventhal and Threkeld, 1978). Molecular composition of bitumen also changes with a decrease in saturated hydrocarbons, whereas aromatic and polar hydrocarbons as well as asphaltenes increase (Zumberge et al., 1978; Forbes et al., 1988; Kříbek et al., 1999; Court et al., 2006). In addition, aromaticity increases with uranium content, for example at Cluff Lake (Landais, 1993), as aromatic hydrocarbons are more stable than aliphatic hydrocarbons in the presence of ionising radiation (Bovey, 1958).

Intensive radiolysis may cause polymerization and condensation of functionalized lipids thus reducing the amount of aliphatics in altered bitumen (Lewan et al., 1991; Landais, 1996b and references therein). A proposed mechanism for this is by the crosslinking of hydrocarbons due to interaction with a free radical. This free radical is produced from the loss of a hydrogen atom with the absorption of radiation energy. When a free radical interacts with another hydrocarbon, a hydrogen atom is abstracted and a C-C bond is formed. Such a mechanism may continue until alkanes and long-chain polymers are rendered infusible (Lewan and Buchardt, 1989; Lewan et al., 1991). Another mechanism that causes polymerization of hydrocarbons is gradual construction from methane (Court et al., 2006).

1.2 Geological Setting

Uranium mineralization in the Cenozoic Narnoo Basin of Western Australia is concentrated towards the end of a paleochannel within the Yilgarn Craton (Fig. 1a). The area has a semi-arid to arid climate with erratic rainfall accumulating 220 mm annually and has a mean daily maximum temperature of 34° C and minimum of 18° C in January, whereas in July the maximum is at 16° C and minimum at 6° C (Douglas et al., 2003). The deposit has not been exposed to temperatures above 50° C. The sediments within the Narnoo Basin were deposited in the Late Mid-Eocene to Late Eocene between the Lower and Upper levels of the Gunbarrel Basin deposits (Fig. 1b; Douglas et al. 2011). Uplift of the Yilgarn Carton during

the Eocene resulted in the lowering of the stream base level and increased stream gradients to form inset valleys that incised into the lower parts of the Gunbarrel Basin (Douglas et al. 2011). During the Miocene or later, regional uplift caused significant weathering of Eocene sediments.

The Mulga Rock sedimentary sequence consists of three terrestrial sedimentary packages defined by Douglas et al. (2011) as: (i) a basal fluviatile sand and gravel; (ii) lacustrine to paludal kaolinitic claystone, peat, clay-rich peat and carbonaceous sand, silt and claystone; and (iii) an upper kaolinitic paludal clay acting as a redox boundary. Uranium and other elements are enriched below the redox front, particularly in the upper 1 to 2 m of the peat and carbonaceous claystone (Douglas et al., 2011). Particulate or discrete mineralogical phases containing uranium are extremely rare. Uranium is mostly amorphously disseminated into a carbonaceous matrix and commonly too fine to be resolved by optical or electron microscopy techniques. Analysis of the rare and ultrafine-grained minerals in scanning electron microscope identified coffinite [$U(SiO_4)_{1-x}(OH)_{4x}$] and uraninite [UO_2] and noted unidentified sulfides associated with high uranium concentrations (Douglas et al., 2011).

2. METHODS

Six samples were collected from the Ambassador Uranium prospect drill core 5766 (Fig. 1a) between 53 to 58.5 m of sedimentary units. Uranium concentrations were measured in the field using a handheld Niton Xlt3 X-Ray Fluorescence (XRF) unit (Fig. 1b).

2.1 Bulk geochemical analyses

The samples were stored at 4° C prior to analysis. Following oven drying at 50° C (three days), samples were powdered finely with a pestle and mortar. About 25 mg of homogenized powder was tested for carbonate by adding hydrochloric acid (HCl, 1M). None of the samples effervesced in HCl indicating absence of carbonate. The powdered samples were then

analyzed for total organic carbon (TOC), nitrogen (TN), and sulfur (TS) contents in an Elementar III Elemental Analyser without further pre-treatment. Another 100 mg aliquot of each powdered sample was analysed by Rock-Eval using a VINCI Rock Eval-II^{+} instrument.

2.2 Organic Petrography

A Leica DM4000 reflected light microscope with 20 x and 50 x objectives was used for the petrographic analyses, reflectance analyses, maceral analysis and photomicrographs. The microscope was equipped with two Baseler digital cameras (b/w and colour), white light and blue light illumination for white reflected light and fluorescence mode. The microscopes components are operated using the software FOSSIl (Hilgers Technisches Buero, Koenigswinter, Germany). White light and fluorescence illumination at excitation wavelengths of 365 and 405 nm was used. The analyses were performed according to ISO7404-3 (2009) and 7404-5 (2009). As the individual samples did not contain sufficient particulate organic matter for reliable maceral analyses, a composite maceral count was performed integrating all six samples.

2.3 Molecular analyses

About 5 g of dry sample material was weighed into a dichloromethane (DCM) pre-extracted glass fibre thimble and ultrasonically extracted (3 x 15 minutes) in an ice bath with DCM. Fresh DCM was used for each sonication cycle. The total extract was concentrated to ~3 mL by evaporating the solvent under a nitrogen purge. Activated Cu powder was added to the total extracts (48 hr) to remove elemental sulfur.

The total extract was filtered through a Pasteur pipette with pre-extracted cotton wool and DCM-rinsed $MgSO_4$ to remove fine CuS, salts, and residual water. The total extract was dried and weighed, and 50% aliquot of the total extract was adsorbed onto pre-activated (120° C for 8 hours) silica gel. The pre-adsorbed sample was loaded onto a silica gel chromatography column (50 mm length x 5 mm diameter), which were pre-cleaned with *n*-

hexane. Saturated, aromatic and polar fractions were eluted using 2 mL solvent mixtures of *n*-hexane, 8:2 (v/v) *n*-hexane: DCM, and 1:1 (v/v) DCM: methanol (MeOH), respectively.

In order to separate the ketones, the polar fraction was adsorbed onto silica gel. The dried sorbate was placed on top of a *n*-hexane pre-rinsed potassium hydroxide (KOH)-impregnated silica gel (20 g KOH dissolved in MeOH per 80 g silica gel). MeOH was removed by rotary evaporation. The ketones were eluted with 2 mL 1:1 (v/v) *n*-hexane: DCM and the remaining polar fraction with 1:1(v/v) MeOH: DCM.

2.4 Instrumentation

Saturated hydrocarbons and ketones were injected splitless *via* an autosampler into a 6890 gas chromatograph (GC) equipped with a DB-5MS column (60 m x 0.25 mm i.d x 0.25 µm film thickness) and interfaced to an HP 5973 mass selective detector. Helium was used as carrier gas (1 mL/min). The saturated hydrocarbon were dissolved in hexane for injection and the GC oven temperature was ramped from 40° C at 3°C /min to 310° C, which was held for 30 minutes. The ketone fraction was dissolved in DCM and the GC oven temperature was ramped from 40° C at 10° C/min to 200° C. The heating rate was decreased to 2° C/min and held at this rate to 320° C, which was held for 30 minutes. Operated in electron ionization mode using 70 eV, masses were scanned from *m/z* 50 to 500 Daltons.

3. RESULTS

3.1 Lithology

Samples were collected from loosely consolidated mid-Eocene carbonaceous sediments from 53 to 58.5 m. The colours of the sediments also reflect their relative characteristic as reduced or oxidized (Fig. 1b). The reduced deposits are carbonaceous dark brown to black clay at depths of 53 to 55 m, which transitions into very fine-grained sand coated with brown to black clay from 56 to 57.5 m, which is overlain by carbonaceous dark brown to black clay

between 57.5 to 59 m. The reduced deposits are capped by leached, kaolinitic white clay at depths of 51 to 52 m, representing a redox front that is defined by the distinct shift from oxidized reddish sands above 48.5 m to highly reduced carbonaceous clays from 53 to 55 m. Mineralization is present in the reduced layers where Uranium concentrations range from barren or background (<200 ppm) to high intermediate (>1700 ppm) with the highest concentration of 5280 ppm in the upper 1 m of the carbonaceous deposit.

3.2 Petrographic analyses

Humotelinite (Sykorova et al., 2005) is rare in this sample set, its presence however allows for determination of the thermal maturity of the carbonaceous shale. The mean random reflectance of eu-ulminite, which is equivalent to vitrinite reflectance of more mature sediments is R_r=0.26 % (based on 50 measurements with a standard deviation of 0.05 %).

A composite maceral analysis performed over all five samples (see Methods) revealed huminite as the predominant type of particulate OM. It is present mainly in the form of attrinite, a maceral of the maceral subgroup detrohuminite, characterizing humic matter that forms a porous groundmass (Sykorova et al., 2005). This attrinitic groundmass contains most of the liptinite and very fine-grained mineral matter (Fig. 2a). Samples contain rare bright metal ores, probably sulfides (Fig. 2 a, b), but optical identification of individual uranium ore minerals was not possible due to their small size or amorphous character.

The liptinites (Taylor et al., 1998) consist predominantly of sporinite, cutinite and fragments of these liptodetrinite (Fig. 2b). Resinite is rare, and alginite is not present in the samples. Amongst inertinitic macerals, only a few fungal spores (funginite) were found, along with traces of semifusinite and fusinite.

On a mineral matter free basis (mmf [%]), the maceral composition is 90.1 vol % huminite with 89.8 % attrinite and 0.3 % ulminite. The liptinite content is 9.9 %, of which the major component is 7 % liptodetrinite with lesser sporinite (1.2 %, Fig. 2d) cutinite (0.8 %),

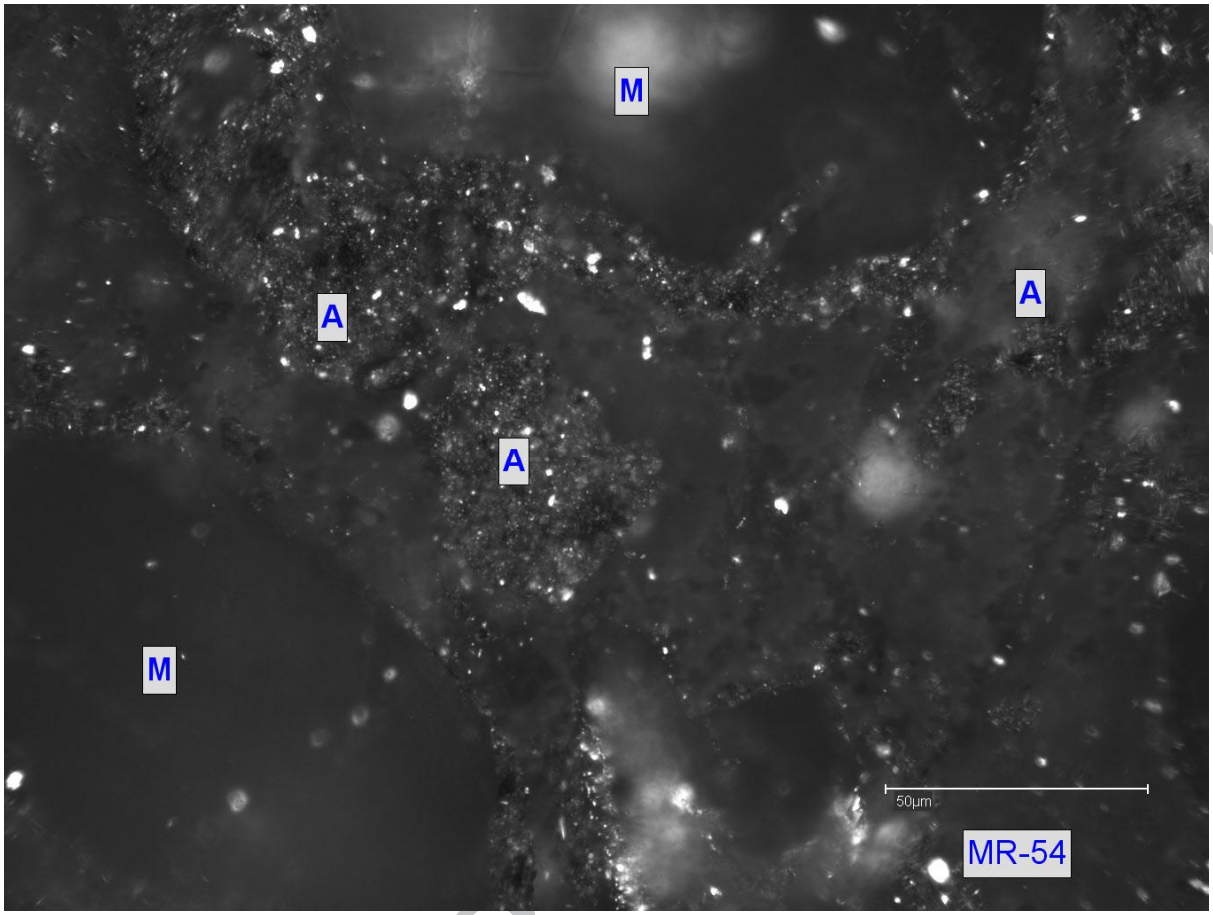

Figyre 2a

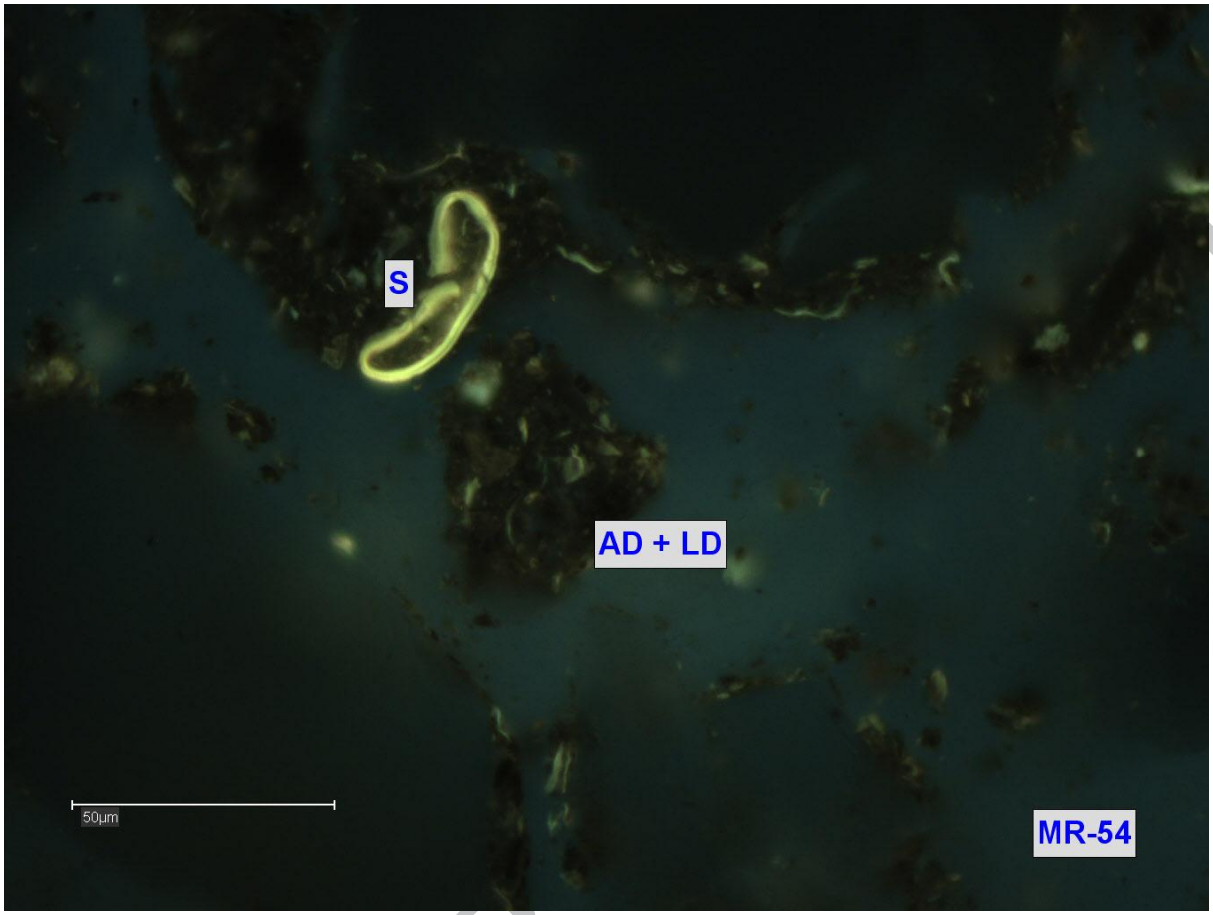

Figyre 2b

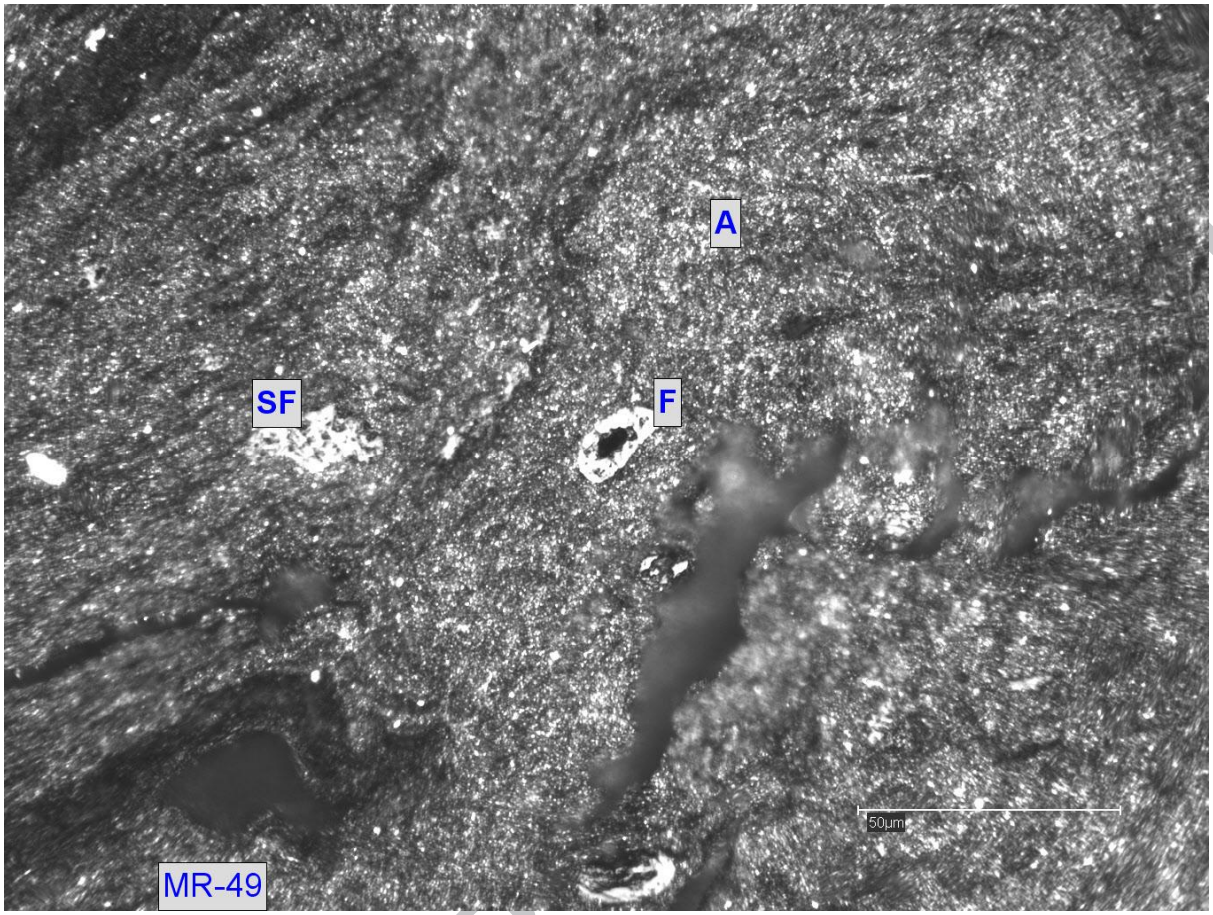

Figyre 2c

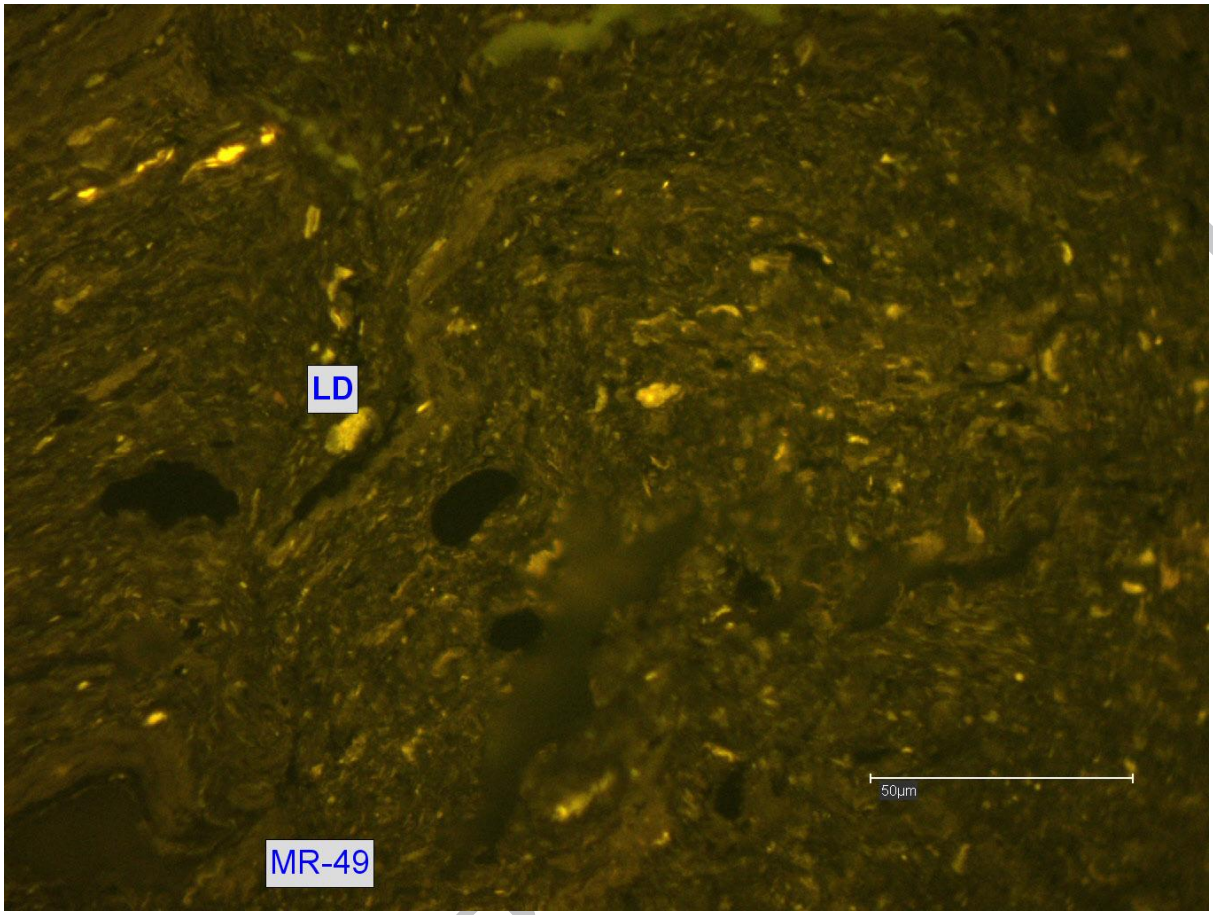

Figyre 2d

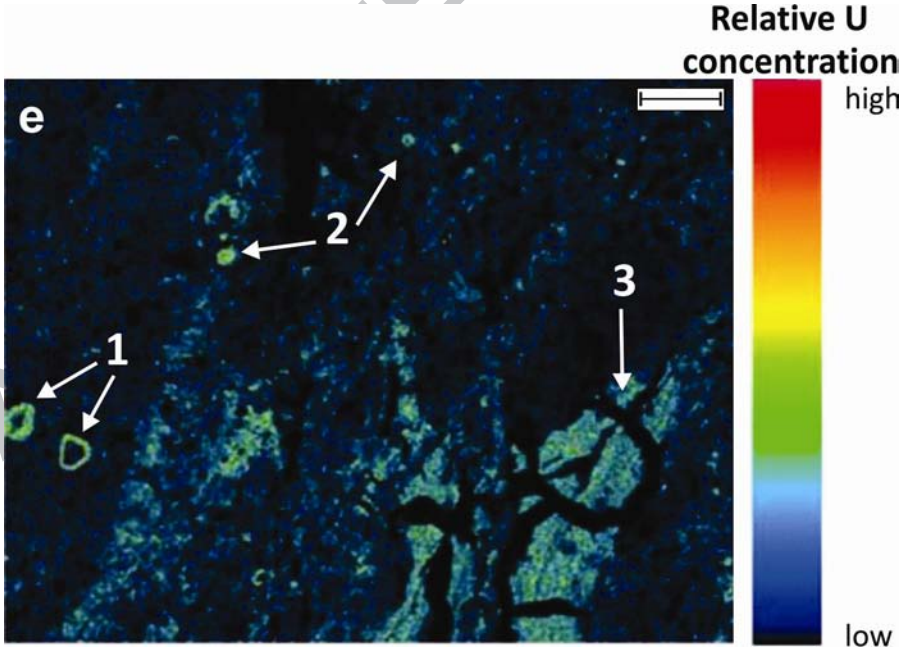

Figyre 2e

and resinite (0.3 %), and trace amounts (<1 %) of funginite, semifusinite and fusinite. This maceral distribution compares well with data from 9 coal seams from the Ambassador deposit, quoted here with permission from Energy and Minerals Australia. The coal was analysed for this company by the same laboratory used by us, and assays 67.5 to 92.3 % attrinite, and 0.5 to 5.6 % telohuminite and ulminite. The liptinite content of the coal is generally comparable with those of the carbonaceous shale with 5.6 to 16.0 % assays; however detritic macerals (liptodetrinite) are less frequent (1.1 to 6.6 %), whereas well-preserved liptinites (sporinite, cutinite, resinite and minor proportions of suberinite) are predominant. About 4 % alginite was noted in one sample of coal, indicating that fragments of alginite may constitute a small proportion of the liptodetrinite in the carbonaceous shale.

The macerals in the samples are clearly of terrestrial origin. Evidence of the effect of radiation on the optical properties of some of the particulate organic matter could not be detected in white light or fluorescence mode.

3.3 Bulk OM composition

A summary of measured bulk parameters is listed in Table 1. Based on our organic petrographic results, we conclude that the particulate OM accumulated in the carbonaceous shale is of terrigenous origin. The bulk composition of the kerogen is a mixture of Type-III or derived from woody, and Type I, which are from non-woody parts of terrigenous plants (e.g. cuticle, spores, and minor amounts of Type-I kerogen from aquatic algae and bacteria). This mixture of biological input from different sources is reflected in the HI and OI values (Fig. 3a). These define a hydrogen-rich (HI of 577 mg hydrocarbon/g TOC) and oxygen-poor (OI of 35 mg CO_2/g TOC) end-member from a hydrogen poor (HI of 292 mg hydrocarbon/g TOC) and oxygen-rich (OI of 69 mg CO_2/g TOC) end-member, with the five samples that have <1700 ppm U forming a mixing line between these two end-members (Fig. 3a). Sample MR-49 deviates from this trend because of a reduced HI-value of 316 mg hydrocarbon/g

Table 1. Bulk, elemental composition and kerogen properties

drill core	depth from surface	CODE	U†	TOC avg	N_{org} ₮	C/N	TS avg	C/S	Extracted bitumen	S1*	S2**	S3***	Tmax	S2/S3	Hydrogen Index, HI	Oxygen Index, OI
	(m)		(ppm)	(%)	(%)		(%)		(wt % of rock)	(mg HC/ g rock)		(mg CO_2/ g rock)	(°C)		(mg HC/ g TOC)	(mg CO_2/ g TOC)
5766	53-53.5	MR 49	5,280	15.1	0.18	84	3.12	5	0.04	0.3	48	7.7	416	6.2	316	51
5766	54-54.5	MR 53	1,700	21.8	0.19	115	1.48	15	1.69	5.9	83	13.8	419	6.0	380	63
5766	55.5-56	MR 50	642	15.9	0.10	161	1.14	14	0.76	2.2	92	5.6	421	16.5	577	35
5766	56.5-57	MR 51	1,161	20.7	0.14	149	1.29	16	1.13	3.3	92	10.5	418	8.7	443	51
5766	57-57.5	MR 54	173	1.6	0.02	148	0.21	8	1.74	0.4	5	1.1	411	4.2	292	69
5766	58-58.5	MR 52	686	12.6	0.09	147	1.15	11	0.37	5.0	50	6.6	414	7.6	397	52

† measured from handheld XRF; ₮ N_{org} is calculated from subtracting N intercept (0.054%) of the linear regression equation from TN; * volatile HC; **pyrolysable HC; *** CO_2 content

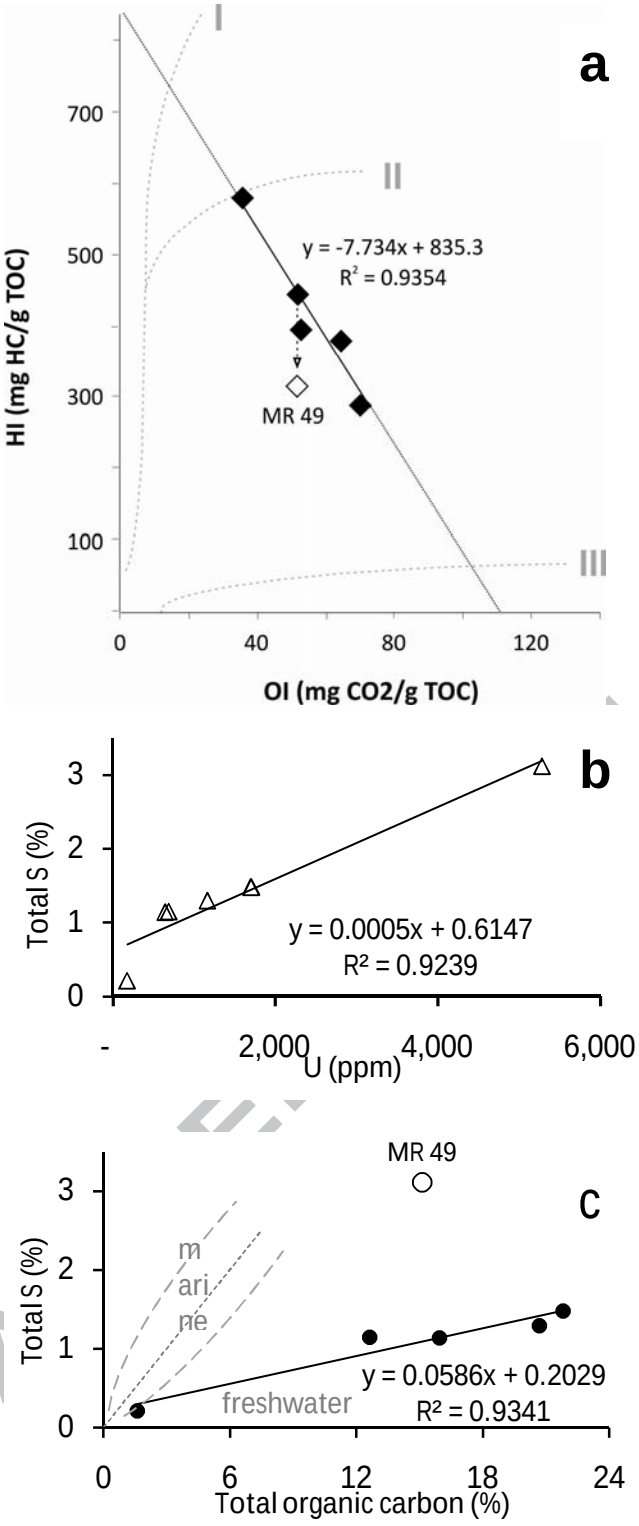

Figyre 3

TOC, when based on its OI value it should give at least 440 mg hydrocarbon/g TOC (as indicated by the origin of the arrow from the mixing line). The lower HI-value of this sample is not caused by a lower quantity of OM (Table 1) and stronger syn-sedimentary oxidation, but attributed to secondary alteration *via* U mineralization.

The four samples MR-50, MR-51, MR-52 and MR-54 with low uranium concentrations reveal a strong linear correlation (R^2=0.9943) between TOC and organic N (N_{org}). The TN intercept of the linear regression trend-line at 0.054 % is used to subtract inorganic N for calculation of N_{org} (Table 1). High C/N values are similar for the four samples and indicate terrigenous sources of OM, whereas C and N values are distinctly low (84 and 115, respectively) in samples with higher uranium concentrations (i.e. MR-49 and MR-53).

The U concentrations versus Total Sulfur (TS) plot in Fig. 3b reveal a trend of covariance with R^2=0.9239, although this is taken with caution as there is a wide gap of representative samples from intermediate U concentrations. The C/S ratios of 5 to 16 are characteristic for non-marine sources (Table 1; Berner and Raiswell, 1984), which are depleted in sulfate (Fig. 3c). MR-49 has an anomalously high-S content compared to the other samples.

3.4 Molecular composition

3.4.1 *n-Alkane distributions*

The aliphatic hydrocarbon composition of the carbonaceous mud is dominated by long chain *n*-alkanes with an odd-over-even predominance (Fig. 4). This is typically observed in mud deposited in lacustrine, paludal, swampy, riverine depositional environments receiving substantial terrigenous input mixed with variable amounts of algal and microbial contributions. This setting is indicated by the high abundance of the 17α(H)-21β(H)-20*R*-homohopane, which is characteristic of peaty and swampy environments with low-pH values even at low degrees of relative thermal maturity (Peters et al., 2005). The aliphatic lipid

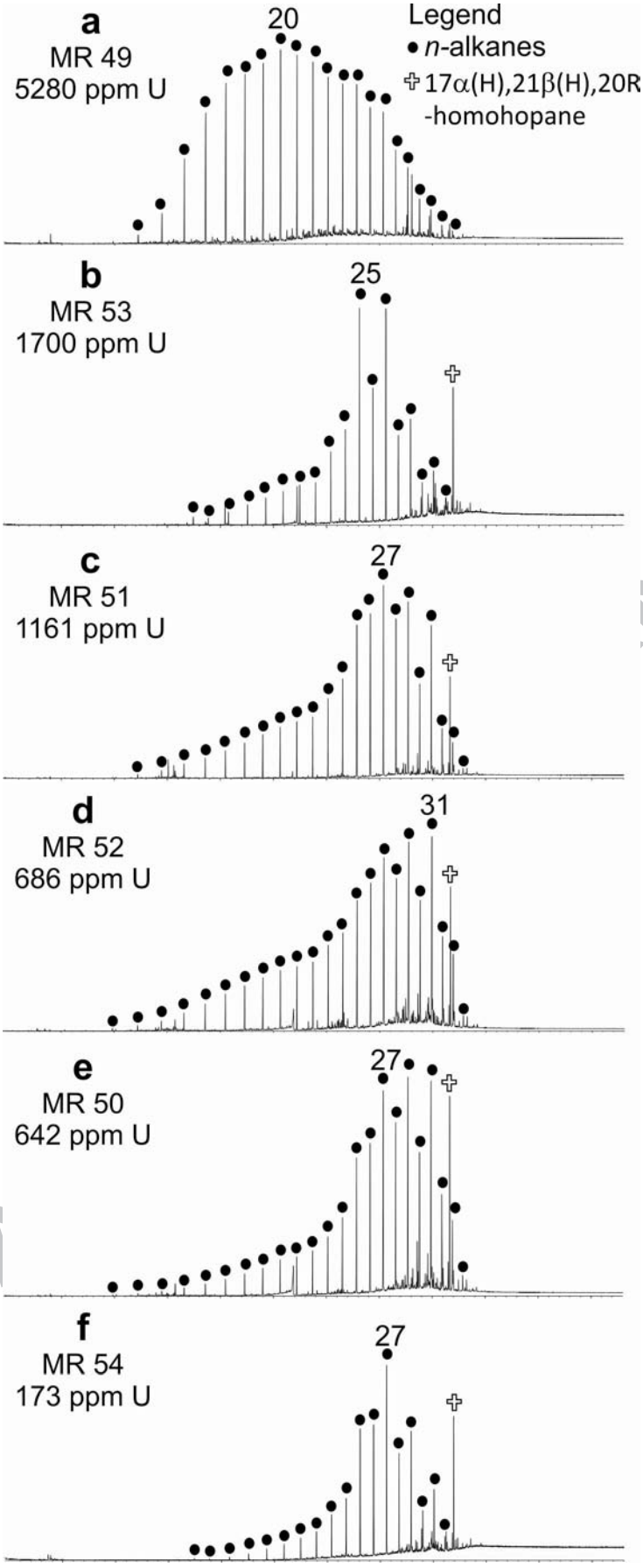

Figyre 4

pattern is consistent with the interpreted depositional environment for the Mulga Rock host-rocks, and the organic petrographic analyses of the OM revealing high proportions of terrigenous and liptinitic macerals.

The two most U enriched samples MR-53 and MR-49 show deviations in the aliphatic hydrocarbon distribution from the other samples, and these cannot be attributed to differences in burial history (Figs. 4a, b). Thermal maturity of these samples was not affected by external heat sources (*e.g.* intrusions) and no differences in degree of weathering or microbial degradation are discernible. This warrants investigation of the aliphatic hydrocarbon distribution in conjunction with U-enrichment. Compared to samples MR-51, MR-52, MR-50, and MR-54, the *n*-alkane distribution of MR-53 reveals a shift in the long chain *n*-alkane distribution from a typical mixed vegetation derived wax lipid pattern dominated by C_{27} to C_{33} towards an *n*-alkane signature dominated by the *n*-C_{25} homologue. This is at the expense of longer chain components, which decline relative to the 17 α (H)-21 β (H)-20*R*-homohopane (Figs. 4b-f). It is noteworthy that the most severe alteration in the aliphatic hydrocarbon pattern is noted in sample MR-49 (Fig. 4a), which also has the highest U concentration. The most abundant *n*-alkane for this sample is *n*-C_{20}. Isoprenoids, present in low concentrations in the remaining samples, and the 17 α (H)-21 β (H)-20*R*-homohopane are reduced to trace amounts. No other isoprenoidal or cyclic alkanes have been identified in the aliphatic hydrocarbon fraction of this particular sample. The absence of an unresolved complex mixture rules out a microbial origin for these aliphatic hydrocarbons (Peters et al., 2005).

3.4.2 n-Alkanone distribution

In the carbonaceous shale investigated here, a series of C_{13}- to C_{33}-alkanones was detected exhibiting multiple ketone positions between C_2 to at least C_{10} in the alkyl chain (Figs. 5 and 6a). Long-chain (C_{25} to C_{31}) alkanones with odd-even-predominance are

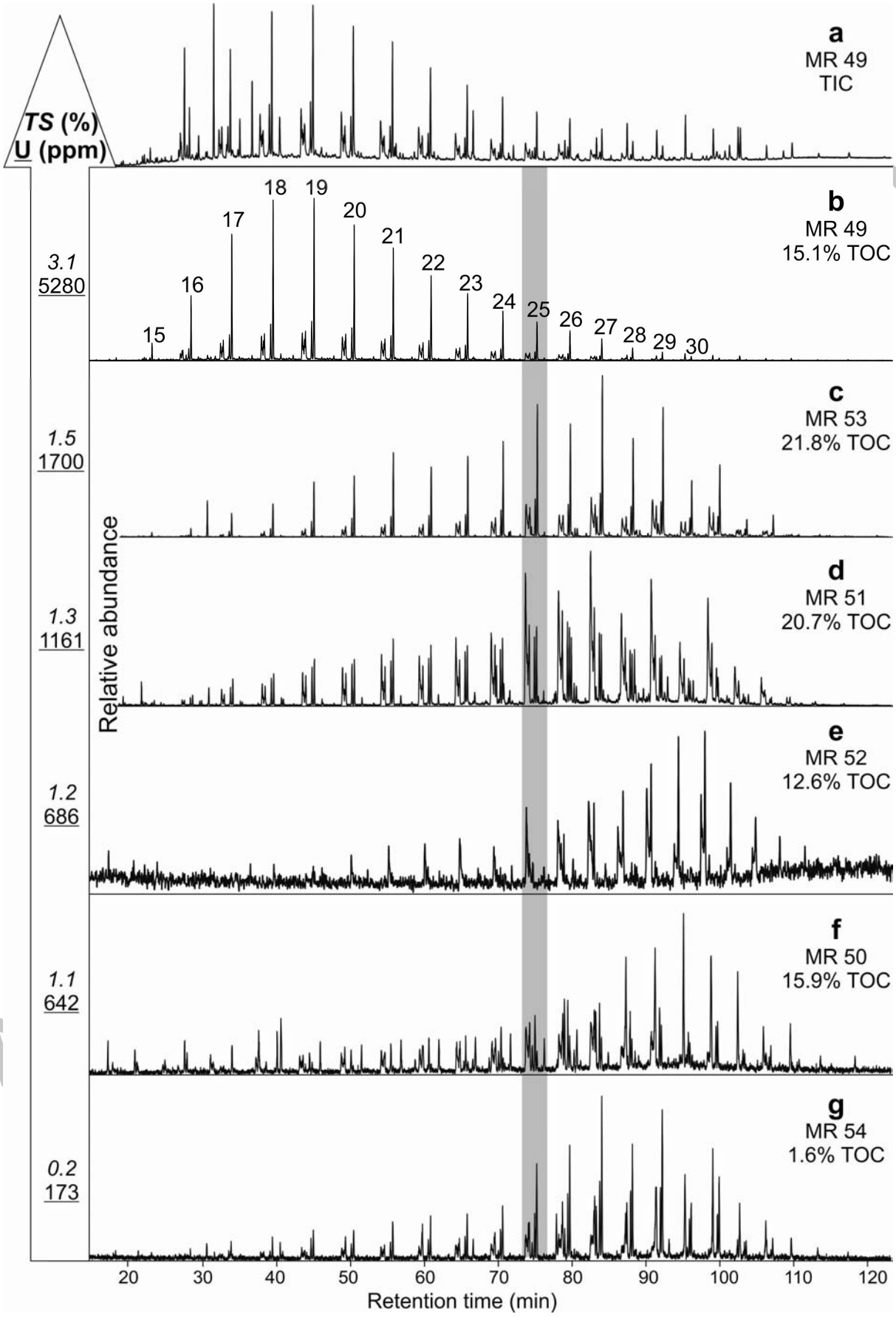
TS (%)
U (ppm)
a
MR 49
TIC
b
MR 49
15.1% TOC
3.1
5280
15
16
17
18
19
20
21
22
23
24
25
26
27
28
29
30
c
MR 53
21.8% TOC
1.5
1700
d
MR 51
20.7% TOC
1.3
1161
Relative abundance
e
MR 52
12.6% TOC
1.2
686
f
MR 50
15.9% TOC
1.1
642
g
MR 54
1.6% TOC
0.2
173
20
30
40
50
60
70
80
90
100
110
120
Retention time (min)

Figyre 5

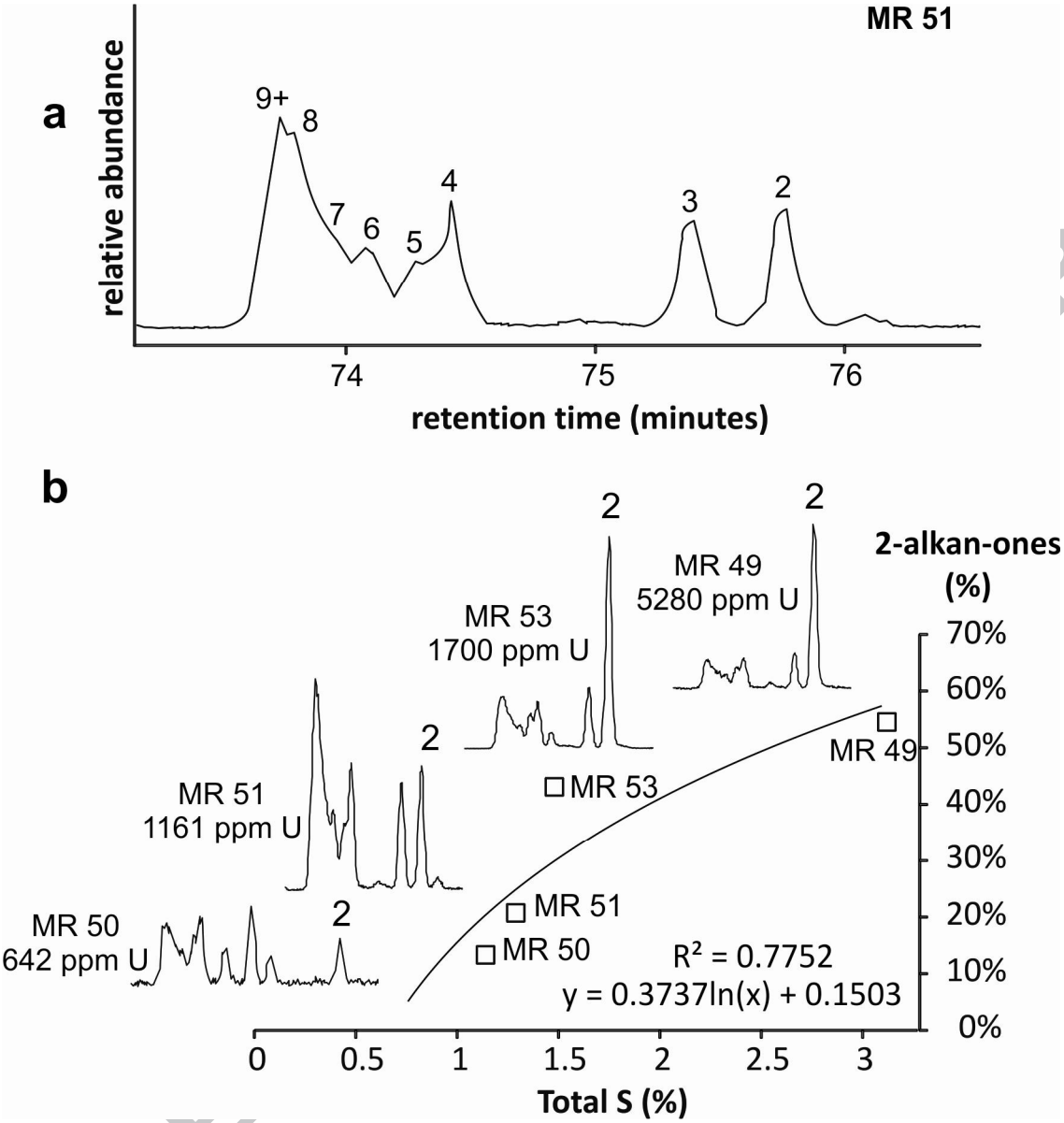
a
MR 51
relative abundance
9+
8
7
6
5
4
3
2
74
75
76
retention time (minutes)
b
MR 51
1161 ppm U
MR 50
642 ppm U
MR 53
1700 ppm U
MR 49
5280 ppm U
2-alkan-ones
(%)
70%
60%
50%
40%
30%
20%
10%
0%
MR 49
MR 53
MR 51
MR 50
R² = 0.7752
y = 0.3737ln(x) + 0.1503
0
0.5
1
1.5
2
2.5
3
Total S (%)

Figyre 6

abundant particularly for samples MR-50, MR-51, MR-52, and MR-54 (Fig. 5d-g), similar to the *n*-alkane distributions. The alkanone mode shifts from C_{27} in the four previous samples to C_{19} in MR-49, with MR-53 hinting at a transition (Fig. 5b, c) thus mimicking changes in chain length of the *n*-alkane distribution. Alkanone concentrations in samples MR-52 and MR-54 are low and the distribution patterns may be affected by analytical bias such as the instrumental resolution (e.g. instrumental resolution; Fig. 5e, g). Samples MR-49, MR-53, MR-51, and MR-50 contain high abundances of alkanones and the distribution patterns reveal significant variation in chain length and in proportion of terminal versus internal alkanones (Fig. 6b).

4.0 DISCUSSION

4.1 Sources and overprinting of n-alkanes

The increase in sample MR-49 of exclusively short to medium chain-length *n*-alkanes (C_{13} to C_{24}), with no odd- or even-predominance indicates their likely generation from a polyaliphatic biopolymer with exclusively straight chain *n*-alkyl moieties. Thermal maturation leading to cracking of C-C bonds in this biopolymer can be excluded due to lack of a heat source and hence radiolytic cleavage of alkyl chains from the biopolymer is invoked, supported by the elevated concentrations of 5280 ppm U in the sample. The *n*-alkenes generated by radiolytic cracking of the biopolymer will then have been protonated rapidly in a low pH environment with abundant hydrogen present. The lack of *n*-alkenes in the sample may indicate that the process of radiolytic cracking took place at rates lower than the hydrogenation potential and/or that the cracking process may have reached an optimum already. Although the depositional age of the sediments at Ambassador is Eocene, the age of the uranium emplacement is less well constrained and may vary between several millions of years to thousand years before present (Douglas et al., 2011). Determining the timing of

mineralization is a challenge in Mulga Rock because the system has remained open and homogenized rendering complications in using isotopic clocks. The redox front and groundwater levels have also moved considerably forming a diverse suite of minerals obliterating most of the primary and diagenetic fabric that is critical in reconstructing the evolution of the deposit (Douglas et al., 2011). A possible estimate of uranium accumulating more efficiently than its removal is during periods of extensive weathering due to humid events in the past 300,000 years (Douglas et al., 2011). This estimate is based on the most predominant disequilibrium pattern if uranium excess, position of the redox front, which is likely a consequence of groundwater level (Douglas et al., 2011).

4.2 Sources and overprinting of alkanones

A variety of *n*-alkanones has been reported from recent and ancient depositional environments and they have been attributed to a multitude of potential sources. A direct plant origin, preferentially from sphagnum species, has been inferred frequently for the *n*-alkan-2-ones (e.g. Volkman et al., 1981; Lehtonen and Ketola, 1990, 1993; Vioque et al., 1996; Baas et al., 2000; Xie et al., 2004; Nichols and Huang, 2007; Zheng et al., 2007; Ortiz et al., 2010; Ortiz et al., 2011). Long chain *n*-alkanones with oxygen functionality in the C_3 to C_9 positions are not present in plants, but alkan-3-ones were reported from aerosol particles and longer mid-chain odd carbon *n*-alkanones of C_{29} to C_{39} from higher plant waxes (Baker, 1974; Cranwell, 1984; Simoneit et al., 1988, 1991; Jetter et al., 2006; Schwark, 2009). Short chain *n*-alkan-3-ones are present rarely in soils, whereas *n*-alkan-2-ones are often abundant (Bai et al., 2006). The alkanone distributions reported in extant land plants is not sufficient to explain the patterns and shifts observed for carbonaceous shale at Ambassador, indicating that their presence and distribution is not strictly depositional.

In addition to a direct plant origin, long (C_{23} to C_{33}) and short (C_{14} to C_{24}) chain *n*-alkanones found in soil, peat and sediments may arise as by-products of microbial

degradation through: (i) microbial oxidation of the corresponding *n*-alkanes (Arpino et al., 1970; Cranwell et al., 1987; Ambles et al., 1993; Jaffé, 1993; van Bergen et al., 1998; Ortiz et al., 2010, 2011); or (ii) microbial beta- oxidation and decarboxylation of *n*-fatty acids (Volkman et al., 1981; Chaffee et al., 1986; De Leeuw, 1986; Quenea et al., 2004). The sediments at Ambassador, however, do not contain keto-bearing isoprenoids that are commonly observed when microbially mediated oxidation of aliphatic, alcohol or fatty acid precursors is considered. This is in agreement with the distribution of aliphatic hydrocarbons (Fig. 4), which also lack isoprenoidal analogues and strongly suggests an origin from a precursor polymer that contained only straight chain alkyl moieties.

Humification may also change the distribution of *n*-alkanones by increasing the relative abundance of short-chain homologues, although a specific mechanism has not yet been elucidated (Lehtonen and Ketola, 1990; Quenea et al., 2004). The shift in the distribution of alkanones in peat materials to a predominantly C_{17}- or C_{21} alkan-2-one, as documented by Lehtonen and Ketola (1990), does not fit the patterns of change observed for the carbonaceous sediments at Ambassador, thus humification cannot sufficiently explain the case of alkanone distribution for this study.

In fossiliferous sediments of higher thermal maturity, *n*-alkan-2-ones are occasionally present and are commonly associated with a thermal evolution of host sediments subjected to volcanic intrusions (e.g. George and Jardine, 1994), formation of hydrothermal petroleum (e.g. Leif et al., 1992; Leif and Simoneit, 1995), or altered bitumen and oil coupled with Mississippi Valley Type metal deposits (e.g. Wu et al., 2012; Wu, 2013). Jurassic oil from the Siberian Platform have been shown to contain *n*-alkan-2-ones accompanied by various oxygenated aromatic hydrocarbons (Strelnikova and Serebrennikova, 2011). Tuo and Li (2005) reported alkanones oxygenated in positions C_2 to C_5 in an outcropping immature Jurassic coal, although it remains unclear whether potential microbial oxidation took place

syn-genetically or through recent weathering of this deposit. Alkan-2-ones have been encountered in exclusively sedimentary environments, whereas samples characterized by intimate thermal overprinting of OM showed exceptional occurrence of alkanones with oxygen functionalities in both terminal and internal chain positions of C_4 to C_9 (e.g. George and Jardine, 1994; Leif and Simoneit, 1995). Such alkanones were also observed in pyrolysis experiments of oil shale and the position of the ketone moiety (C_2 to C_{12}) was interpreted to indicate a former ether-bonding site to the kerogen network (e.g. van de Meent et al., 1980; Sinninghe Damsté et al., 1993; Riboulleau et al., 2000). Thermally induced cleavage of ether bonds as observed in pyrolysis experiments may thus contribute to the formation particularly of mid-chain alkanones.

There are frequent reports of alkanones with various oxygenation positions between C_3 to C_{10}, usually dominated by alkan-9-ones and alkan-10-ones when derived from *Botryococcus braunii*-type algae, generated upon pyrolysis of the ether cross-linked algal biopolymer (Gatellier et al., 1993; Sinninghe Damsté et al., 1993). There are, however, no reports of mid-chain ether bond *n*-alkyl lipids in sporinite so far and hence this formation mechanism remains unproven. The carbonaceous sediments at Ambassador have neither been buried significantly nor affected by heat sources such as intrusions, and consequently a thermal formation of C_2 to C_{10} keto-substituted alkanes is unlikely.

The conversion to alkanones of long chain carboxylic acids present as free molecules is not a valid pathway for our samples, because the carbonaceous sediments at Ambassador do not contain long chain fatty acids. Previous pyrolysis treatment of sporinite generated a suite of terminal monocarboxylic acids ranging from C_9 to C_{33} and maximising at C_{13} (Blanc et al., 1991). Carboxylic acids released from the biopolymers could subsequently undergo partial reduction to yield the *n*-alkan-2-one distribution found in the carbonaceous sediments at Ambassador. Exclusively terminal carboxylic acids forming upon sporinite pyrolysis and

migration of carboxylic moiety along the alkyl chain is also not feasible, thus making an origin of the alkan-3-ones to alkan-9-ones observed from sporinite carboxylic acids unlikely. Previous work on liptinitic oil shale by Regtop et al. (1982, 1985) pointed towards an origin of alkan-2-ones via decarboxylation of β-ketoesters, but indicated that formation of mid-chain analogues according to this model is not possible.

Thus, none of the previously-observed source or causality for alkanones can sufficiently explain the patterns of their distribution in the Ambassador deposits. Taking note that the abundance of alkanones and the alkan-2-one isomer increase with higher U content of the bulk sample opens a strong possibility that alkanone production is a result of radiolysis as we discuss below.

4.3 Uranium localization

The U-concentration within our samples is generally non-uniform as shown in Fig. 2e. Enrichment of U has been noted in palynomorphs possessing poly-aliphatic exine biopolymers (e.g. Bubert et al., 2002; de Leeuw et al., 2006), in particular spores and pollen (but not excluding fungal or bacterial palynomorphs), which we have also determined by maceral analyses (Section 3.2). The intimate spatial association of an amorphous U-coating with the biopolymers of the palynomorph is postulated to initiate radiolytic cleavage of alkyl-lipids from the macromolecules, ultimately forming the suite of alkanones observed. Several potential pathways of formation are discussed in the following section.

4.4 Mechanism of alkanone formation

Analogous to thermal cracking as documented by George and Jardine (1994) and Leif and Simoneit (1995), it is feasible to assume that radiolytic cleavage of alkyl chains from a poly-aliphatic biopolymer will yield in the first instance terminal alkenes (Fig. 7). These may undergo rapid isomerization of the double bonds through acid catalysis leading to various

positional alkene isomers that may subsequently undergo hydration to intermittently give the corresponding alcohols, which are very rapidly dehydrogenated to form the more stable alkanones (Leif and Simoneit, 1995). The high hydrogen concentration in the low pH peaty environment of the sediments at Ambassador may have facilitated intensive alkene isomerization. Depending on the prevailing degree of alkene isomerization, alkanones with keto-functionalities between C_3 to C_{10} can be formed. In early stages of radiolytic cracking, alkyl-chains with biologically inherited odd-carbon-predominance may be generated and these will undergo intensive isomerization leading to a diverse suite of alkanones, which will produce similar abundances of alkanone isomers as observed for sample MR-51 (Fig. 6b). Experiments conducted by Leif and Simoneit (1995) on the Messel Oil Shale in Germany with 1-hexadecene and eicosane spiked into the substrate yielded an evenly distributed alkanone isomers mixture comparable to the hydrothermal oil in the Guaymas Basin in California. Similar results have been obtained here on bitumen extracts from Mulga Rock samples MR-50, MR-51, and MR-53 (Figs. 5d, f and 6b).

The sample with the highest U-content and hence the potentially highest radiolytic alteration of an aliphatic biopolymer precursor at Ambassador gives a distribution that differs from the other, less U-rich samples (MR-49; Fig. 5b). The isomer pattern is dominated by the alkan-2-ones and a trend towards the alkan-2-one dominance is already indicated in sample MR-53, characterized by the 1700 ppm U-concentration (Table 1; Figs. 5c and 6b). When conducting hydrous pyrolysis experiments, Leif and Simoneit (1995) tested for the effects of catalytic additives in the formation of alkanones and noted that in the presence of iron sulfide the distribution of alkanones generated was dominated by the alkan-2-one with lesser contributions from other isomers. This observation is confirmed in the sedimentary sequence at Mulga Rock where Sample MR-49, having a sulfur content almost three times higher than the other samples (Table 1; Fig. 5b) and contains iron sulfides (Douglas et al., 2011), reveals

an alkanone distribution strongly dominated by the alkan-2-one isomer. The decline in the chain length of the alkanones in Sample MR-49 is due to successive radiolytic cracking of alkyl chains from the aliphatic biopolymer precursor thus leaving only shorter alkyl moieties for cleavage in the advanced stage of radiolytic alteration.

The high U-content in the Ambassador sample will concomitantly lead to radiolytic cleavage of water molecules, yielding highly reactive OH^- radicals that will rapidly interact with the double bond of the alkenes produced simultaneously (Fig. 7). This may lead to a fast formation of the corresponding alkanones, then preferably in the alkan-2-one configuration due to insufficient time for double bond migration, as observed for Sample MR-49. Thus, for the first time, it can be proven in the natural setting and at a molecular level that radiolysis can yield characteristic alkanone degradation products at average sediment levels of only 1000 to 5280 ppm U. Localized enrichment of U within these sediments may, however, cause much higher-dose levels.

The proposed formation mechanism involves α-radiation induced cleavage of alkyl side chains from aliphatic biopolymers forming the outer exine of palynomorphs to yield terminal alkenes, which can undergo double bond isomerization in the low pH, peaty environment. Subsequent reaction of either OH^- radicals, formed through water radiolysis in U-rich sediments, with the alkenes yielded ketones or alternatively alkenes (Fig. 7). The alkanones would then be hydrogenated to alcohols, which when dehydrogenated can revert to alkanones. Depending on the location of the double bond in the alkene precursor, alkanones with keto functionalities in the corresponding positions will result. Suppression of double bond isomerization and hence preferential formation of alkan-2-ones is favored in sulfur-rich environments, particularly those bearing iron sulfides, and by rapid reaction of alk-1-enes with OH^- radicals prior to double bond migration.

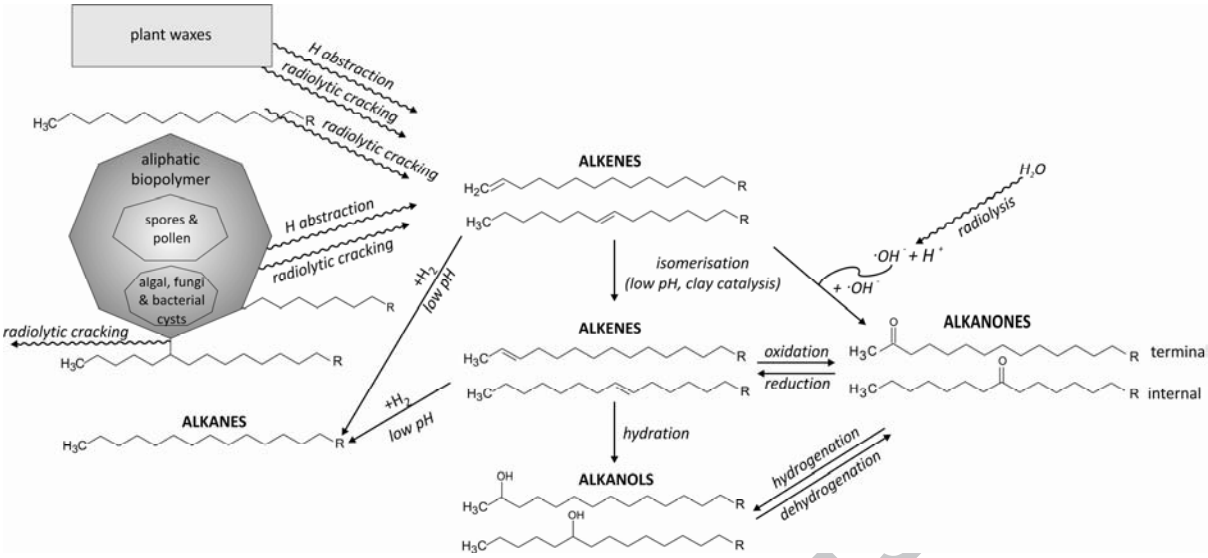

Figyre 7

4.5 Effects of radiolysis on OM

Uranium enrichment and associated radiation will affect the composition of sediment OM by reducing the relative proportion of hydrogen (as monitored by HI or the H/C ratio) or dehydrogenation and in parallel increase the oxygen proportion (OI or O/C ratio kerogen) in the bulk kerogen or black shale (Zumberge et al., 1978; Nakashima et al., 1984; Leventhal et al., 1986; Dahl et al., 1988; Lewan and Buchardt, 1989; Disnar and Sureau, 1990; Landais, 1996b; Court et al., 2006; Greenwood et al., 2013). Most of the radiation resulting from ^{238}U decay in natural systems will be emitted in the form of α-radiation (Lewan et al., 1991), which has a shallow penetration depth of <100 microns, followed by less intensive γ-radiation which penetrates several decimeters. In natural systems it must be noted that distribution of radiation-emitting elements is not uniform and hence intimate spatial association of OM and U can lead to significant alteration despite the shallow penetration depth of α-rays. Petrographic evidence for α-radiation damage has been reported frequently (see review in Landais, 1996).

In natural sedimentary systems and oils, the effect of ionizing radiation on a molecular level reduces the amount of isoprenoids versus *n*-alkanes and causes side chain cleavage in steroids (Dahl et al., 1988). A decline in the ratio of long chain versus short chain alkanes with increasing U-content indicates radiolytic cracking of hydrocarbon chains (Dahl et al., 1988). Upon radiolysis normal alkanes loose H-atoms approximately three times more rapidly from a secondary position than from a primary position (Wojnarovits and Schuler, 2000). Loss from the different secondary positions is essentially statistical with competing processes involved in bond rupture producing radicals in the radiolysis of normal alkanes. The formation of alkenes due to radiolytic decay has been shown for a number of natural oils (Frolov, 1995).

Several experiments that have artificially applied radiation to natural OM have been conducted (e.g. Lewan et al., 1991), based on the use of γ-radiation that might not be representative for near natural conditions where α-radiation is of higher relevance. No formation of ketones was observed in these artificial radiolysis experiments. However, intentional routine radiolytic treatment to fresh food and plant materials for sterilization purposes in food processing does result in formation of other alteration products. These radiolytic products, such as *n*-alkenes, have been observed after the radiolytic treatment of peanuts (Park and Hwang, 1999), apricots and herbs (Kim et al., 2010). *n*-Alkanes and *n*-alkenes from meat-derived triglycerides (Barba et al., 2012) have been reported as well as the formation of volatile aromatic compounds (Kim et al., 2005), and various alkyl lipids, including cyclobutanones (Blanch et al., 2009; Crews et al., 2012). Radiolytic cracking of heavy oils and bitumen has been demonstrated to be feasible, although the generation of light hydrocarbons is counterbalanced by heavy polymerization products (Lewan et al., 1991; Zaikin, 2008; Zaikin and Zaikina, 2013).

Based on the above listed references, ample evidence exist that even upon moderate irradiation intensity, alteration of lipids and organic biopolymers can proceed in a fashion similar to that observed in carbonaceous mud at Ambassador. The degree of alteration may vary with respect to radiation dose, duration of radiation exposure, spatial association of U and affected organics and other parameters. The main products of radiolytic alteration in this study are straight-chain alkanes and alkanones, which exhibit a similar distribution pattern (Figs. 4 and 5).

In samples with low uranium concentrations of <1700 ppm, long chain alkyl lipids with a predominance of odd-numbered chain length isomers provides an original record of depositional terrestrial plant origin and confirms low thermal maturity for the system. The alkyl lipid signature is consistent with the bulk kerogen composition, the organic petrology

results and the sedimentological characteristics of the depositional environment. Slight alteration of the alkyl lipid composition is noted in Sample MR-53, where the mode of *n*-alkane isomers is shifted from a C_{27}+C_{29}+C_{31} cluster to C_{25} dominance and in the alkanones fraction, where a shift in the isomer pattern towards a dominance of the alkane-2-one is recognized (Figs. 4b and 6). Much stronger alteration is present in sample MR-49, in agreement with a threefold higher U-concentration, which has experienced the same thermal history compared to the other samples. The massive shift in *n*-alkanes towards shorter chain analogues, accompanied by a complete loss of odd-over-even predominance, indicates carbon-carbon bond cracking of higher molecular weight *n*-alkanes and massive addition of newly formed *n*-alkanes without a wax-inherited odd-over-even predominance. The lack of isoprenoidal compounds generated by this cracking process suggests a poly-aliphatic precursor devoid of isoprenoidal structural moieties. This excludes microbial OM as a potential source and indicates an origin from polyaliphatic biopolymers, making spore exines or algeanan the most suitable precursors. The absence of alginite in micropetrographical analysis accompanied by a high abundance of sporinite and the U-enrichment on sporinite palynomorphs supports a radiolytic breakdown of the sporinite-type biopolymer to yield the corresponding straight chain alkanes and eventually alkanones.

5.0 CONCLUSIONS

A close spatial association of amorphous U and phytoclast surfaces induced radiolytic cracking of highly aliphatic biopolymers producing *n*-alkanes is present at the Ambassador U prospect, Mulga Rock. Radiolysis and a cascade of secondary and tertiary reactions, such as further cracking, radiolysis of water to produce OH^- radicals and carbonylation, produced a suite of terminal and mid-chain alkanones. The diversity of alkanone isomers decreases and their distribution is dominated by the alkan-2-one moiety when isomerization is inhibited by

rapid reaction with radicals, such as OH^-, the latter generated from water radiolysis at high U concentrations. It is shown for the first time that alkanones form as radiolytic degradation products from aliphatic biopolymers at bulk amorphous uranium concentrations ≥1700 ppm. Low radiation doses associated with <5000 ppm U and geologically short exposure times possibly during the last 300,000 years prevented formation of radiolytic haloes. Such haloes are usually observed where U concentration in the organic matter is much higher and radiation exposure is much longer the U concentrations and exposure times of organic matter from our study. Tracking "radiolytic molecular markers" can serve as an early tool for radiolysis in instances where petrographic and mineral alteration is not discernible.

The breaking of C-C bonds in low temperature and pressure systems, much lower than those observed in the oil window, and recognition of radiolytic effects can have implications regarding initiation of petroleum formation, paleo-environmental reconstructions, mineral exploration, and environmental applications. Thus in addition to biogenic, anthropogenic and petrogenic molecular markers, we propose that "radiolytic molecular markers" can be indicative of radiolytic cracking rather than thermal or microbial oxidation.

ACKNOWLEDGEMENTS

Australia's Commonwealth Scientific and Industrial Research Organization provided funding for this study through a flagship program on the Organic Geochemistry of Mineral Systems. We thank Australian Research Council and John de Laeter Centre for infrastructure and Geoff Chidlow and Lyndon Berwick for technical support.

REFERENCES

Alexandre, P., Kyser, T.K., 2006. Geochemistry of uraniferous bitumen in the southwest Athabasca basin, Saskatchewan, Canada. Econ. Geol. 101, 1605-1612.

Ambles, A., Jambu, P., Jacquesy, J.C., Parlanti, E., Secouet B., 1993. Changes in the ketone portion of lipidic components during the decomposition of plant debris in a hydromorphic forest-podzol. Soil Sci. 156, 49-56.

Anderson, R.F., 1987. Redox behavior or uranium in an anoxic marine basin. Uranium 3, 145-164.

Arpino, P., Albrecht, P., Ourisson, G., 1970. Series homologues aliphatics dans un sediment Eocène d'origen lacustre. Comptes Rendus Acad. de Sci., Series D 270, 1760–1763.

Baas, M., Pancost, R., van Geel, B., Sinninnghe-Damsté, J.S., 2000. A comparative study of lipids in Sphagnum species. Org. Geochem. 31, 535-541.

Bai, Y., Fang, X., Wang, Y., Kenig, F., Miao, Y., Wang, Y., 2006. Distribution of aliphatic ketones in Chinese soils: Potential environmental implications. Org. Geochem. 37, 860-869.

Baker, E.A., 1974. The influence of environment on leaf wax development in *Brassica oleracea var. gemmifera*. New Phytol. 73, 955-966.

Barba, C., Santa-Maria, G., Herraiz, M., Calvo, M.M., 2012. Rapid detection of radiation-induced hydrocarbons in cooked ham. Meat Sci. 90, 697-700.

Behrends, T., Van Cappellen, P., 2005. Competition between enzymatic and abiotic reduction of uranium(VI) under iron reducing conditions. Chem. Geol. 220, 315-327.

Berner, R.A., Raisewell, R., 1984. C/S method for distinguishing freshwater from marine sedimentary rocks. Geol. 12, 365-368.

Blanc, P., Valisolalao, J., Albrecht, P., Kohut, J. P., Muller, J.F., Duchene, J.M., 1991. Comparative geochemical study of three Maceral Groups from a high-volatile bituminous coal. Energ. Fuel. 5, 875-884.

Blanch, G.P., Caja, M.D., Flores, G., del Castillo, M.L.R., 2009. Identification of 2-dodecylcyclobutanone and linear-alkanes as irradiation markers in sliced dry-cured ham. Food Chem. 113, 616-620.

Breger, I.A., 1974. The role of organic matter in the accumulation of uranium. In: International Atomic Energy Agency (Ed.), Formation of uranium deposits. International Atomic Energy Agency, Athens, Greece, 99-123.

Bubert, H., Lambert, J., Steuernagel, S., Ahlers, F., Wiermann, R., 2002. Continuous decomposition of sporopollenin from pollen of *Typha angutifolia L.* by acidic methanolysis. Verlag der Zeitschrift für Naturforschung 57c, 1035-1041.

Chaffee, A.L., Hoover, D.S., Johns, R.B., Schweighardt, F.K., 1986. Biological markers extractable from coal. In: Johns, R.B. (Ed.), *Biological Markers in the Sedimentary Record.* Elsevier, Amsterdam. pp. 311-345.

Court, R.W., Sephton, M.A., Parnell, J., Gilmour, I., 2006. The alteration of organic matter in response to ionising irradiation: Chemical trends and implications for extraterrestrial sample analysis. Geochim. Cosmochim. Acta 70, 1020-1039.

Cranwell, P.A., 1984. Alkyl esters, mid chain ketones and fatty acids in late glacial and postglacial lacustrine sediments. Org. Geochem. 6, 115-124.

Cranwell, P. A., Eglinton, G., Robinson, N., 1987. Lipids of aquatic organisms as potential contributors to lacustrine sediments 2. Org. Geochem. 11, 513-527.

Crews, C., Driffield, M., Thomas, C., 2012. Analysis of 2-alkylcyclobutanones for detection of food irradiation: Current status, needs and prospects. J. of Food Compos. Analysis 26, 1-11.

Dahl, J., Hallberg, R., Kaplan, I.R., 1988. Effects of irradiation from uranium decay on extractable organic-matter in the Alum Shales of Sweden. Org. Geochem. 12, 559-571.

de Leeuw, J.W., 1986. High molecular weight markers. In: Johns, R.B. (Ed.) *Biological Markers in the Sedimentary Records*. Elsevier, Amsterdam, pp. 256-258.

de Leeuw, J.W., Versteegh, G.J.M., Bergen, P.F.V., 2006. Biomacromolecules of algae and plants and their fossil analogues. Plant Ecol. 182, 209-233.

Disnar, J.R., Sureau, J.F., 1990. Organic-matter in ore genesis - Progress and Perspectives. Org. Geochem. 16, 577-599.

Douglas, G. B., Butt, C. R. M., Gray, D. J., 2003, Mulga Rock Uranium and multielement deposits, Officer Basin, WA. In: Butt, C.R.M., Robertson, I.D.M., Scott, K.M., Cornelius, M. (Eds.) Regolith expression of Australian ore systems. CRC LEME, Perth, pp 415-417.

Douglas, G. B., Butt, C.R.M., Gray, D.J., 2011. Geology, geochemistry and mineralogy of the lignite-hosted Ambassador palaeochannel uranium and multi-element deposit, Gunbarrel Basin, Western Australia. Mineralium Deposita 46, 761-787.

Forbes, P., Landais, P., Bertrand, P.E.B., Espitalie, J., Yahaya, M., 1988. Chemical transformations of type-III organic matter associated with the Akouta uranium deposits (Niger): geological implications. Chem. Geol. 71, 267-282.

Frolov, E.B., 1995. Alkene/Alkane correlations within olefin-containing Paleozoic crude oils from Oklahoma and Texas. *Org. Geochem.* 23, 447-450.

Gatellier, J.P.L.A., de Leeuw, J.W., Sinninghe Damsté, J.S., Derenne, S., Largeau, C., Metzger, P., 1993. A comparative-study of macromolecular substances of a Coorongite and cell-walls of the extant alga *Botryococcus Braunii*. Geochim. Cosmochim. Acta 57, 2053-2068.

George, S.C., Jardine, D.R., 1994. Ketones in a Proterozoic dolerite sill. Org. Geochem. 21, 829-839.

Gizė, A.P., 2000. The organic geochemistry of Gold, Platinum, Uranium and Mercury deposits. In: Giordano, T.S., Kettler, R.M., Wodd, S.A. (Eds.), Ore genesis and exploration: the roles of organic matter. Society of Econ. Geologists, Inc., Colorado, pp. 217-250.

Goldhaber, M.B., Hemingway, B.S., Mohagheghi, A., Reynolds, R.L., Northrop, H.R., 1987. Origin of coffinite in sedimentary rocks by a sequential adsorption-reduction mechanism. Bull. de Miner. 110, 131-144.

Greenwood, P.F., Brocks, J.J., Grice, K., Schwark, L., Jaraula, C.M.B., Dick, J.M., Evans, K.A., 2013. Organic geochemistry and mineralogy. I. Characterisation of organic matter associated with metal deposits. Ore Geol. Rev. 50, 1-27.

Halbach, P., Vonborstel, D., Gundermann, K.D., 1980. The uptake of uranium by organic-substances in a peat bog environment on a granitic bedrock. Chem. Geol. 29, 117-138.

Idiz, E.F., Carlisle, D., Kaplan, I.R., 1986. Interaction between organic matter and trace metals in a uranium rich bog, Kern County, California, U.S.A. Appl. Geochem. 1, 573-590.

Ilger, J.D., Ilger, W.A., Zingaro, R.A., Mohan, M.S., 1987. Modes of occurrence of uranium in carbonaceous uranium deposits - characterization of uranium in a South Texas (USA) Lignite. Chem. Geol. 63, 197-216.

ISO7404-3, 2009. Methods for the petrographic analysis of coals – Part 3, Method of determining maceral group composition.

ISO7404-5, 2009. Methods for the petrographic analysis of coals – Part 5, Method of determining microscopically the reflectance of vitrinite.

Jaffé, R., 1993. On the origin and fate of n-alkane-2-ones in freshwater environments. In: Manning, D. (Ed.), Organic Geochemistry: Applications in Energy and the Natural Environment. Manchester University Press, Manchester, pp. 356-359.

Jeon, B.H., Dempsey, B.A., Burgos, W.D., Barnett, M.O., Roden, E.E., 2005. Chemical reduction of U(VI) by Fe(II) at the solid-water interface using natural and synthetic Fe(III) oxides. Environ. Sci. Technol. 39, 5642-5649.

Jetter, R., Kunst, L., Samuels, A.L., 2006. Composition of plant cuticular waxes. In: Riederer, M., Mueller, C. (Eds.), Annual Plant Reviews: Biology of the Plant Cuticle, Blackwell, Oxford, pp. 145-181.

Kim, H., Cho, W.J., Ahn, J.S., Cho, D.H., Cha, Y.J., 2005. Identification of radiolytic marker compounds in the irradiated beef extract powder by volatile analysis. Microchem. J.80, 127-137.

Kim, M.J., Ki, H.A., Kim, W.Y., Pal, S., Kim, B.K., Kang, W.S., Song, J.M., 2010. Development of radiation indicators to distinguish between irradiated and non-irradiated herbal medicines using HPLC and GC-MS. Anal. Bioanal. Chem. 398, 943-953.

Kříbek, B., Za,k K., Spangenberg, J., Jehlicka, J., Prokes, S., Kominek, J., 1999. Bitumens in the late Variscan hydrothermal vein-type uranium deposit of Pribram, Czech Republic: Sources, radiation-induced alteration, and relation to mineralization. Econ. Geol. 94, 1093-1114.

Landais, P., 1993. Bitumens in uranium deposits. In: Parnell, J., Landais, P. (Eds.), Bitumens in Ore Deposits. Springer-Verlag, Berlin, pp. 213-238.

Landais, P., 1996. Organic geochemistry of sedimentary uranium ore deposits. Ore Geol. Rev. 11, 33-51.

Landais, P., Connan, J., Dereppe, J.M., George, E.F., Meunier, J.D., Monthioux, M., Pagel, M., Pironon, J., Poty, B., 1987. Alterations of the organic matter, a clue for uranium ore genesis. Uranium 3, 307-342.

Lehtonen, K., Ketola, M., 1990. Occurrence of long-chain acyclic methyl ketones in Sphagnum and Carex peats of various degrees of humification. Org. Geochem. 15, 275-280.

Lehtonen, K., Ketola, M., 1993. Solvent-extractable lipids of Sphagnum, Carex, Bryales and Carex Bryales peats - content and compositional features vs peat humification. Org. Geochem. 20, 363-380.

Leif, R.N., Simoneit, B.R.T., 1995. Ketones in hydrothermal petroleums and sediment extracts from Guaymas Basin, Gulf of California. Org. Geochem. 23, 889-904.

Leif, R.N., Simoneit, B.R.T., Kvenvolden, K.A., 1992. Hydrous pyrolysis of *n*-$C_{32}H_{66}$ in the presence and absence of inorganic components in the American Chemical Society Division of Fuel Chemistry 204th National Meeting Preprints 37, pp. 1748-1753.

Leventhal, J. S., Threlkeld, L. N., 1978, Carbon-13/carbon-12 isotope fractionation of organic matter associated with uranium ores induced by alpha radiation: Science, v. 202, p. 430-432.

Leventhal, J.S., Daws, T.A., Frye, J.S., 1986. Organic geochemical analysis of sedimentary organic matter associated with uranium. Appl. Geochem. 1, 241-247.

Leventhal, J.S., Grauch, R.I., Threlkeld, C.N., Lichte, F.E., 1987. Unusual organic matter associated with uranium from the Claude Deposit, Cluff Lake, Canada. Econ. Geol. 82, 1169-1176.

Lewan, M.D., Buchardt, B., 1989. Irradiation of organic-matter by uranium decay in the Alum Shale, Sweden. Geochim. Cosmochim. Acta 53, 1307-1322.

Lewan, M. D., Ulmishek, G. F., Harrison, W., and Schreiner, F., 1991. Gamma ^{60}Co-irradiation of organic matter in the Phosphoria Retort Shale: Geochim. Cosmochim. Acta 55, 1051-1063.

Lovely, D.R., Phillips, E.J.P., Gorby, Y.A., Landa, E.R., 1991. Microbial reduction of uranium. Nature 350, 413-416.

Meunier, J. D., Landais, P., and Pagel, M., 1990, Experimental-Evidence of Uraninite Formation from Diagenesis of Uranium-Rich Organic-Matter: Geochim. Cosmochim. Acta, 54, 809-817.

Mohagheghi, A., Updegraff, D.M., Goldhaber, M.B., 1984. The role of sulfate-reducing bacteria in the deposition of sedimentary uranium ores. Geomicrobiol. J.4, 153-173.

Nakashima, S., Disnar, J.-R., Perruchot, A., Trichet, J., 1984. Experimental study of mechanisms of fixation and reduction of uranium by sedimentary organic matter under diagenetic or hydrothermal conditions. Geochim. Cosmochim. Acta 48, 2321-2329.

Nakashima, S., Disnar, J.-R., Perruchot, A., 1999. Precipitation kinetics of uranium by sedimentary organic matter under diagenetic and hydrothermal conditions. Econ. Geol. 94, 990-1006.

Nichols, J.E., Huang, Y.S., 2007. C_{23}-C_{31} *n*-alkan-2-ones are biornarkers for the genus Sphagnum in freshwater peatlands. Org. Geochem. 38, 1972-1976.

Ortiz, J.E., Gallego, J.L.R., Torres, T., Diaz-Bautista, A., Sierra, C., 2010. Palaeo-environmental reconstruction of Northern Spain during the last 8000 cal yr BP based on the biomarker content of the Ronanzas peat bog (Asturias). Organic Geochem. 41, 454-466.

Ortiz, J.E., Diaz-Bautista, A., Aldasoro, J.J., Torres, T., Gallego, J.L.R., Moreno, L., Estebanez, B., 2011. n-Alkan-2-ones in peat-forming plants from the Ronanzas ombrotrophic bog (Asturias, northern Spain). Org. Geochem. 42, 586-592.

Park, J.Y., Hwang, K.T., 1999. Hydrocarbons as markers for identifying postirradiated peanuts. J. Am. Oil Chem. Soc. 76, 125-129.

Peters, E.P., Walters, C.C., Moldowan, J.M., 2005. The Biomarker Guide. Cambridge University press, New York.

Quenea, K., Derenne, S., Largeau, C., Rumpel, C., Mariotti, A., 2004. Variation in lipid relative abundance and composition among different particle size fractions of a forest soil. Org. Geochem. 35, 1355-1370.

Regtop, R.A., Crisp, P.T., Ellis, J., 1982. Chemical characterization of shale oil from Rundle, Queensland. Fuel 61, 185-192.

Regtop, R.A., Ellis, J., Crisp, P.T., Ekstrom, A., Fookes, C.J.R., 1985. Pyrolysis of model compounds on spent oil shales, minerals and charcoal - implications for shale oil composition. Fuel 64, 1640-1646.

Riboulleau, A., Derenne, S., Sarret, G., Largeau, C., Baudin, F., Connan, J., 2000. Pyrolytic and spectroscopic study of a sulphur-rich kerogen from the "Kashpir oil shales" (Upper Jurassic, Russian platform). Org. Geochem. 31, 1641-1661.

Schwark, L., 2009. Hydrocarbons in the Pedosphere. In: Timmins, K. (Ed.), Handbook of Hydrocarbon and Lipid Microbiology I, Springer, New York. pp. 280-295.

Simoneit, B.R.T., Cox, R.E., Standley, L.J., 1988. Organic-Matter of the Troposphere-IV. Lipids in Harmattan aerosols of Nigeria. Atmos. Environ. 22, 983-1004.

Simoneit, B.R.T., Sheng, G.Y., Chen, X.J., Fu, J.M., Zhang, J., Xu, Y.P., 1991. Molecular marker study of extractable organic-matter in aerosols from urban areas of China. Atmospheric Environ. part A-Gen. Topics 25, 2111-2129.

Sinninghe Damsté, J.S., de las Heras, F.X.C., van Bergen, P.F., de Leeuw, J.W., 1993. Characterization of Tertiary Catalan lacustrine oil shales: Discovery of extremely organic sulphur-rich Type I kerogens. Geochim. Cosmochim. Acta 57, 389-415.

Spirakis, C.S., 1996. The roles of organic matter in the formation of uranium deposits in sedimentary rocks. Ore Geol. Rev. 11, 53-69.

Strelnikova, E.B., Serebrennikova, O.V., 2011. Ketones of western Siberian Jurassic oils. Petroleum Chem. 51, 264-269.

Sykorova, I., Pickel, W., Christanis, K., Wolf, M., Taylor, G.H., Flores, D., 2005. Classification of Huminite – ICCP System 1994. International J. Coal Geol. 62, 85-106.

Taylor, G.H., Teichmueller, M., Davis, A., Diessel, C.F.K., Littke, R., Robert, P., 1998. *Organic Petrology*, Borntraeger, Berlin, Stuttgart.

Tuo, J.C., Li, Q., 2005. Occurrence and distribution of long-chain acyclic ketones in immature coals. Appl. Geochem. 20, 553-568.

van Bergen, P.F., Nott, C.J., Bull, I.D., Poulton, P.R., Evershed, R.P., 1998. Organic geochemical studies of soils from the Rothamsted Classical Experiments—IV. Preliminary results from a study of the effect of soil pH on organic matter decay. Org. Geochem. 29, 1779-1795.

van de Meent, D., Brown, S.C., Philp, R.P., Simoneit, B.R.T., 1980. Pyrolysis-high resolution gas chromatography and pyrolysis gas chromatography-mass spectrometry of kerogens and kerogen precursors. Geochim. Cosmochim. Acta 44, 999-1013.

Vioque, J., Pastor, J., Vioque, E., 1996. Leaf wax ketones in the genus Coincya. Phytochem. 42, 1047-1050.

Volkman, J.K., Gillan, F.T., Johns, R.B., Eglinton, G., 1981. Microbial lipids of an inter-tidal sediment .2. Sources of neutral lipids in a temperate inter-tidal sediment. Geochim. Cosmochim. Acta 45, 1817-1828.

Wojnarovits, L., Schuler, R.H., 2000. Bond rupture in the radiolysis of n-alkanes: An application of gel permeation chromatography to studies of radical scavenging by iodine. J.of Phys. Chem. A 104, 1346-1358.

Wu, Y, 2013. The relationship between oil-gas organic matter and MVT mineralization: A case study of the Chipu lead-zinc deposit, Sichuan. Acta Geoscientia Sinica 4, 425-436.

Wu, Y., Wang, Y., Lei, T., Chang, J., Xia, Y., 2012. Possible origin of high molecular weight n-alkan-2-ones in jurassic bitumens from the Sichuan Basin in Southwest China. Chem. Technol. Fuels Oils 48, 195-201.

Xie, S.C., Nott, C.J., Avsejs, L.A., Maddy, D., Chambers, F.M., Evershed, R.P., 2004. Molecular and isotopic stratigraphy in an ombrotrophic mire for paleoclimate reconstruction. Geochim. Cosmochim. Acta 68, 2849-2862.

Zaikin, Y.A., 2008. Low-temperature radiation-induced cracking of liquid hydrocarbons. Radiat. Phys. Chem. 77, 1069-1073.

Zaikin, Y.A., Zaikina, R.F., 2013. Polymerization as a limiting factor for light product yields in radiation cracking of heavy oil and bitumen. Radiat. Phys. Chem. 84, 6-9.

Zheng, Y., Zhou, W., Meyers, P. A., Xie, S., 2007. Lipid biomarkers in the Zoigê-Hongyuan peat deposit: Indicators of Holocene climate changes in West China. Org. Geochem. 38, 1927-1940.

Zumberge, J.E., Sigleo, A.C., Nagy, B., 1978. Molecular and elemental analyses of the carbonaceous matter in the gold and uranium bearing Vaal Reef carbon seams, Witwatersrand Sequence. Mineral Sci. Eng. 10, 223-246.

CAPTIONS

Fig. 1: a) Location of the Mulga Rock uranium district in the Narnoo Basin of Western Australia (star; adapted from Douglas et al., 2011); b) Simplified lithology and stratigraphy of drill hole 5766 from the Ambassador deposit. Symbols: * depth from surface (m); †uranium concentration measured by handheld XRF.

Fig. 2: a) Sample MR-54, attrinite (A) filling pore space between mineral grains (M) – white reflected light; b) Sample MR-54 in fluorescence mode (UV excitation, 365 nm) showing a bright yellow fluorescing sporinite exine; A + Ld = attrinitic groundmass containing liptodetrinite; c) Sample MR-49 under white light; attrinitic groundmass (A), fungal spore (F) and semifusinite fragment (SF); d) Sample MR-49, same field of view as in Fig. 2c in fluorescence mode (405 nm excitation) showing abundant detrital liptinitic organic matter; LD= liptodetrinite; and e) U distribution map of block specimen representative for the Ambassador prospect using field emission electron probe microanalysis. Note preferential U enrichment in palynomorphs (marked by white arrows 1, 2), moderate enrichment in woody organic material (arrow marked 3) and low impregnation of background mineral matrix.

Fig. 3: Bulk organic composition samples from the Ambassador prospect. a) Rock Eval HI versus OI diagram, the five samples with U concentration >1700 ppm depict a mixing line between H-rich/O-poor and H-poor/O-rich components. Sample MR-49 deviated from this trend by HI-values being too low. Origin of the arrow indicates HI value on the mixing line. b) TS versus U concentration reveal a strong linear dependency. c) TS *versus* TOC concentration indicates a sulfur-lean lacustrine depositional environment and highlights anomalous sulfur enrichment in Sample MR-49. C/S associated with marine environments is delineated based on Berner and Raisewell (1984).

Fig. 4: GC/MS total ion current (TIC)-traces of aliphatic hydrocarbons from six core samples from the Ambassador prospect. Most abundant *n*-alkane carbon number is labelled.

Fig. 5: a) GC/MS TIC-trace and (b, c, d, e, f, and g) summed *m/z* 58+72+86+100 mass fragment grams indicative of *n*-alkanones for six core samples from the Ambassador prospect. Isomers of *n*-pentacosanone (grey band) are enlarged in Fig. 6.

Fig. 6: a) Partial chromatogram of *n*-pentacosanone of MR-53 with carbonyl functional groups in positions C2 to C9 (and higher) labelled; and b) The distribution of isomers shifts to a predominance of *n*-alkan-2-ones in samples with high TS contents (e.g. partial chromatograms of *n*-pentacosanones).

Fig. 7: Schematic diagram summarizing and illustrating pathways for alkanone formation upon radiolytic alteration (see text for details).

Highlights:

- Bulk kerogen compositions indicate land plant sources for organic matter in the uranium deposit.
- Radiolysis led to cleavage of straight long chain forming medium chain length *n*-alkyl moieties.
- Secondary and tertiary reactions with $OH^{\cdot}$ radicals promoted the formation of alkanones.
- "radiolytic molecular markers" imply molecular markers resulting from radiolytic cracking.
- A mechanism is proposed for the production of *n*-alkanes and *n*-alkanones

Radiolytic alteration of biopolymers in the Mulga Rock (Australia) uranium deposit

Caroline M.B. Jaraula, Lorenz Schwark, Xavier Moreau, Walter Pickel, Leon Bagas and Kliti Grice

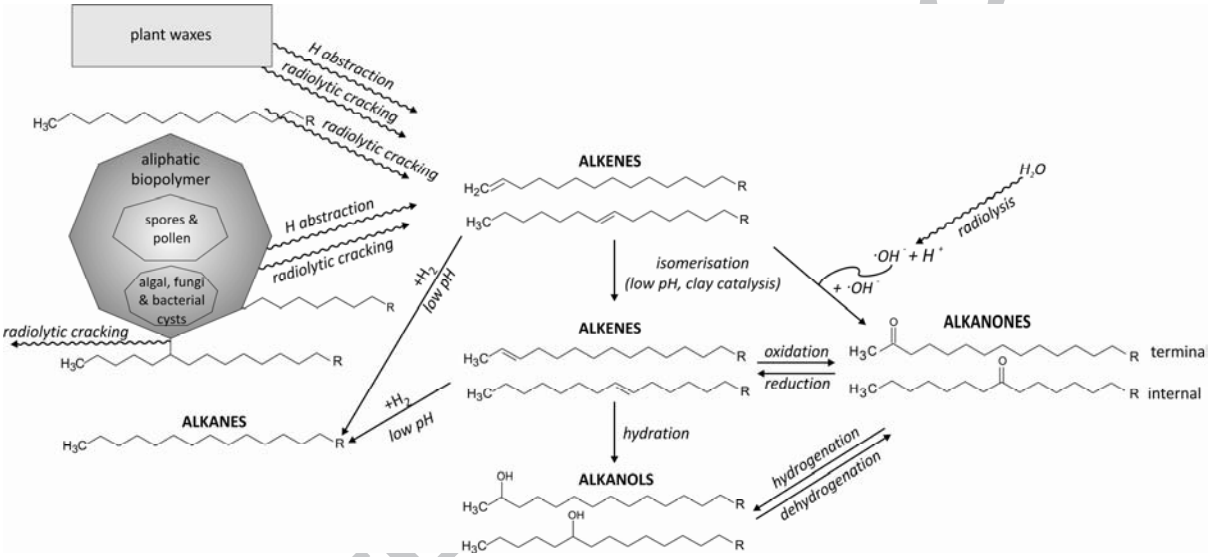

Schematic diagram summarizing and illustrating pathways for alkanone formation upon radiolytic alteration